



# 1 Evaluating reanalysis-driven CORDEX regional climate models 2 over Australia: model performance and errors

3 Giovanni Di Virgilio<sup>1</sup> · Jason P. Evans<sup>1,2</sup> · Alejandro Di Luca<sup>1,2</sup> · Roman Olson<sup>3,4,5</sup> · Daniel Argüeso<sup>6</sup> · Jatin Kala<sup>7</sup> ·  
4 Julia Andrys<sup>7</sup> · Peter Hoffmann<sup>8,9</sup> · Jack J. Katzfey<sup>8</sup> · Burkhardt Rockel<sup>10</sup>

5 Received: 18 September 2018 / Accepted: 6 February 2019  
6 © Springer-Verlag GmbH Germany, part of Springer Nature 2019

## 7 Abstract

8 The ability of regional climate models (RCMs) to accurately simulate current and future climate is increasingly important  
9 for impact assessment. This is the first evaluation of all reanalysis-driven RCMs within the CORDEX Australasia framework  
10 four configurations of the Weather Forecasting and Research (WRF) model, and single configurations of COSMO-CLM  
11 (CCLM) and the Conformal-Cubic Atmospheric Model (CCAM) to simulate the historical climate of Australia (1981–2010)  
12 at 50 km resolution. Simulations of near-surface maximum and minimum temperature and precipitation were compared  
13 with gridded observations at annual, seasonal, and daily time scales. The spatial extent, sign, and statistical significance  
14 of biases varied markedly between the RCMs. However, all RCMs showed widespread, statistically significant cold biases  
15 in maximum temperature which were the largest during winter. This bias exceeded  $-5$  K for some WRF configurations,  
16 and was the lowest for CCLM at  $\pm 2$  K. Most WRF configurations and CCAM simulated minimum temperatures more  
17 accurately than maximum temperatures, with biases in the range of  $\pm 1.5$  K. RCMs overestimated precipitation, especially  
18 over Australia's populous eastern seaboard. Strong negative correlations between mean monthly biases in precipitation  
19 and maximum temperature suggest that the maximum temperature cold bias is linked to precipitation overestimation. This  
20 analysis shows that the CORDEX Australasia ensemble is a valuable dataset for future impact studies, but improving the  
21 representation of land surface processes, and subsequently of surface temperatures, will improve RCM performance. The  
22 varying RCM capabilities identified here serve as a foundation for the development of future regional climate projections  
23 and impact assessments for Australia.

24 **Keywords** CORDEX-Australasia · Dynamical downscaling · Model bias · Precipitation · Temperature

A1 **Electronic supplementary material** The online version of this  
A2 article (<https://doi.org/10.1007/s00382-019-04672-w>) contains  
A3 supplementary material, which is available to authorized users.

A4 ✉ Giovanni Di Virgilio  
A5 giovanni@unsw.edu.au

A6 <sup>1</sup> Climate Change Research Centre, University of New South  
A7 Wales, Sydney, Australia

A8 <sup>2</sup> Australian Research Council Centre of Excellence  
A9 for Climate Extremes, University of New South Wales,  
A10 Sydney, Australia

A11 <sup>3</sup> Department of Atmospheric Sciences, Yonsei University,  
A12 Seoul, Republic of Korea

A13 <sup>4</sup> Center for Climate Physics, Institute for Basic Science,  
A14 Pusan, Republic of Korea

A15 <sup>5</sup> Pusan National University, Pusan, Republic of Korea

<sup>6</sup> Department of Physics, University of Balearic Islands,  
Palma de Mallorca, Spain A16  
A17

<sup>7</sup> School of Veterinary and Life Sciences, Environmental  
and Conservation Sciences, Murdoch University, Perth,  
Western Australia, Australia A18  
A19  
A20

<sup>8</sup> Climate Science Centre-CSIRO Oceans and Atmosphere,  
Aspendale, VIC, Australia A21  
A22

<sup>9</sup> Climate Service Center Germany (GERICS),  
Helmholtz-Zentrum Geesthacht, Hamburg, Germany A23  
A24

<sup>10</sup> Institute of Coastal Research, Helmholtz-Zentrum  
Geesthacht, Geesthacht, Germany A25  
A26

## 1 Introduction

Climate change is a global phenomenon with impacts that manifest at regional and local scales (IPCC 2013). Assessing how these changes will impact physical, ecological, and socio-economic systems and planning response strategies requires robust, high-resolution regional climate projections (IPCC 2012; Rummukainen 2016; Xue et al. 2014). Global climate models (GCMs) provide a basis for this information, however, their coarse resolution lacks the fine-scale details required by the assessment and adaptation planning community (Fowler et al. 2007; Hattermann et al. 2011; Maraun et al. 2010). An effective approach for producing high-resolution climate projections at regional scales is to use regional climate models (RCMs) to dynamically downscale coarse-resolution outputs from GCMs or reanalyses (Giorgi 2006; Laprise 2008; Wang et al. 2004). RCMs use these outputs as initial and lateral boundary conditions to generate projections that better resolve the complex surface characteristics and mesoscale atmospheric processes that are important drivers of regional climate (Di Luca et al. 2012; Giorgi and Bates 1989; Torma et al. 2015). With increased spatial resolution, RCMs can also better resolve convective phenomena and thus improve the simulation of extreme events, such as sub-daily precipitation extremes (Olsson et al. 2015). Accurate simulation of climate extremes by RCMs is increasingly important for climate impact assessment (Halmstad et al. 2013; Sunyer et al. 2017).

The Coordinated Regional Downscaling Experiment (CORDEX) is an initiative of the World Climate Research Programme (WCRP) that aims to improve both the generation and evaluation of downscaled regional climate information (Giorgi et al. 2009). Under the CORDEX framework, regional climate projections based on CMIP5 (Coupled Model Intercomparison Project Phase 5) GCM projections have been produced for 14 regions worldwide. An important stage in RCM development and the production of future regional climate projections is the evaluation of the models' skill in simulating present-day climatological conditions (Di Luca et al. 2016; Diaconescu et al. 2015; Garcia-Diez et al. 2015). In this capacity, an essential component of CORDEX is the evaluation of multiple RCMs over recent decades using lateral boundary conditions from re-analysis products such as ERA-Interim (Dee et al. 2011).

Evaluations of historical CORDEX RCM simulations forced by ERA-Interim reanalysis have been completed for several regions. These assessments generally show that RCMs capture the main climatological features of the target domain; however, deficiencies are present which vary depending on the model, sub-region, and season.

For example, when simulating observed precipitation in Africa, Nikulin et al. (2012) found that RCMs showed marked regional variation, and displayed shortcomings in arid and semi-arid regions. Furthermore, Panitz et al. (2014) reported a dry bias in regions affected by the passage of the West African Monsoon, warm biases in arid regions, and a cold bias over Guinea. RCMs showed reasonably high model accuracy over most of the Middle East and North African domain at annual timescales (Bucchignani et al. 2016). However, a warm summertime bias over North Africa and Saudi Arabia, and a cold bias over the majority of the domain during the boreal winter were also apparent. Evaluations of the EURO-CORDEX domain showed that RCMs simulated the basic spatiotemporal patterns of the European climate. However, model deficiencies included cold and wet biases during most seasons over the majority of Europe and warm and dry summer biases over southern and south-eastern Europe (Kotlarski et al. 2014). Although the general climatological features of South America were reproduced by RCMs, marked wet and cold biases were evident over several regions (Solman et al. 2013).

To date, no evaluation of CORDEX-Australasia has been performed and there is limited information available regarding the capability of ERA-Interim driven RCMs in simulating the Australian climate. While several studies have used RCMs driven with various reanalyses to produce regional climate hindcasts for different regions of the Australian continent (e.g., Evans et al. 2012; Andrys et al. 2015), no intercomparison study has evaluated the relative performance of different RCMs in simulating the Australian climate. Consequently, this paper has three main aims: (1) to evaluate the ability of the CORDEX-Australasia ensemble to simulate the historical temperature and precipitation characteristics of Australia, identifying regions where model biases are common and statistically significant; (2) to assess the relative strengths and weaknesses of individual RCMs; and (3) to assess the possible reasons for deficiencies in model performance. Model evaluation focuses on the entire CORDEX-Australasia ensemble which consists of four configurations of the Weather Research and Forecasting (WRF) model (Skamarock et al. 2008), the COSMO-CLM (CCLM) model (Rockel et al. 2008), and the Conformal-Cubic Atmospheric Model (CCAM; McGregor and Dix 2008). We evaluate the ability of this RCM ensemble to simulate near-surface maximum and minimum air temperature and precipitation at annual, seasonal, and daily time scales over Australia. These variables were chosen because they are often used for impact studies and are well-represented in high-quality gridded observational data sets for the Australian continent (King et al. 2013).

## 128 2 Data and methods

### 129 2.1 Model configurations

130 The RCMs were driven by ERA-Interim boundary conditions with a spatial resolution of approximately 80 km for  
 131 a 29-year period from January 1981 to January 2010. The  
 132 WRF RCM configurations used the Advanced Research  
 133 WRF (ARW) solver which uses a fully compressible,  
 134 Eulerian and non-hydrostatic equation set. It uses terrain-  
 135 following, hydrostatic-pressure for the vertical coordinate,  
 136 which has constant pressure surface at the top of  
 137 the model. The horizontal grid uses Arakawa C-grid stag-  
 138 gering. Its time integration scheme uses the third-order  
 139 Runge–Kutta scheme, with a smaller time step for acoustic  
 140 and gravity-wave modes. Further information on WRF  
 141 can be found in Skamarock et al. (2008). All WRF con-  
 142 figurations used a domain with quasi-regular grid spac-  
 143 ing of approximately 50 km ( $0.44^\circ \times 0.44^\circ$  on a rotated  
 144 coordinate system) covering the CORDEX-Australasia  
 145 region. Model performance was evaluated for Australia  
 146 only (Fig. 1). The four configurations of the WRF RCM  
 147 (UNSW-WRF360J, UNSW-WRF360K, UNSW-WRF360L,  
 148 and MU-WRF330) used different parameterisations  
 149 for planetary boundary layer physics, surface physics,  
 150 cumulus physics, and radiation (Table 1). The UNSW-  
 151 WRF360J, UNSW-WRF360K, and UNSW-WRF360L  
 152 configurations were selected from a larger ensemble of  
 153 WRF RCMs that accurately simulated the south-eastern  
 154 Australian climate, whilst retaining as much independent  
 155 information as possible (Evans et al. 2012, 2014; Ji et al.  
 156 2014). Parameterisations selected for MU-WRF330 were

158 based on results from a prior sensitivity analysis of WRF  
 159 to different physics and input data over southwest Western  
 160 Australia (Kala et al. 2015). The MU-WRF330 simulation  
 161 (Andrys et al. 2015) was conducted using WRF version  
 162 3.3, whereas the three other WRF simulations were con-  
 163 ducted using version 3.6.0.

164 CCAM is a non-hydrostatic, variable-resolution global  
 165 atmospheric model that includes a number of distinctive fea-  
 166 tures. It uses two-time level, semi-implicit time differenc-  
 167 ing and semi-Lagrangian horizontal advection with bi-cubic  
 168 horizontal interpolation. It also incorporates total-variation-  
 169 diminishing (TVD) vertical advection (McGregor 1993) and  
 170 reversible staggering (McGregor and Dix 2008). CCAM  
 171 (version 1209) was run with a global uniform grid configura-  
 172 tion at 50 km resolution and used the setup shown in Table 1.  
 173 When forced with ERA-Interim data, the model setup was  
 174 similar to the setups described in Katzfey et al. (2016) and  
 175 Thevakaran et al. (2016), except that a scale-selective filter  
 176 (i.e., spectral nudging, Thatcher and McGregor 2009) with  
 177 a scale of 9000 km was used every 6 h for temperature,  
 178 winds above approximately 900 hPa, and surface pressure.  
 179 In addition, CCAM used ERA-Interim sea surface tempera-  
 180 tures (SST) rather than the bias and variance corrected SSTs  
 181 developed for CCAM by Hoffmann et al. (2016).

182 The COSMO model in CLimateMode ('CCLM') is a  
 183 non-hydrostatic RCM developed from the Local Model  
 184 (LM) of the German Weather Service. It solves the  
 185 thermo-hydrodynamic equations for compressible flow  
 186 in a moist atmosphere on an Arakawa-C grid which is  
 187 defined on a rotated coordinate system. The vertical grid  
 188 uses a hybrid coordinate that is terrain-following near the  
 189 surface and flat near the top of the model. The standard  
 190 land surface model (LSM) used by CCLM is TERRA-ML

**Fig. 1** Topographic variation across the study domain, Australia. Approximate location of the Great Dividing Range is delineated in white. *NT* Northern Territory, *QLD* Queensland, *NSW* New South Wales, *ACT* Australian Capital Territory, *TAS* Tasmania, *VIC* Victoria, *SA* South Australia, *WA* Western Australia. Inset **a** shows natural resource management (NRM) climate regions (*MDB* Murray Darling Basin). Inset **b** shows the CORDEX Australasia domain

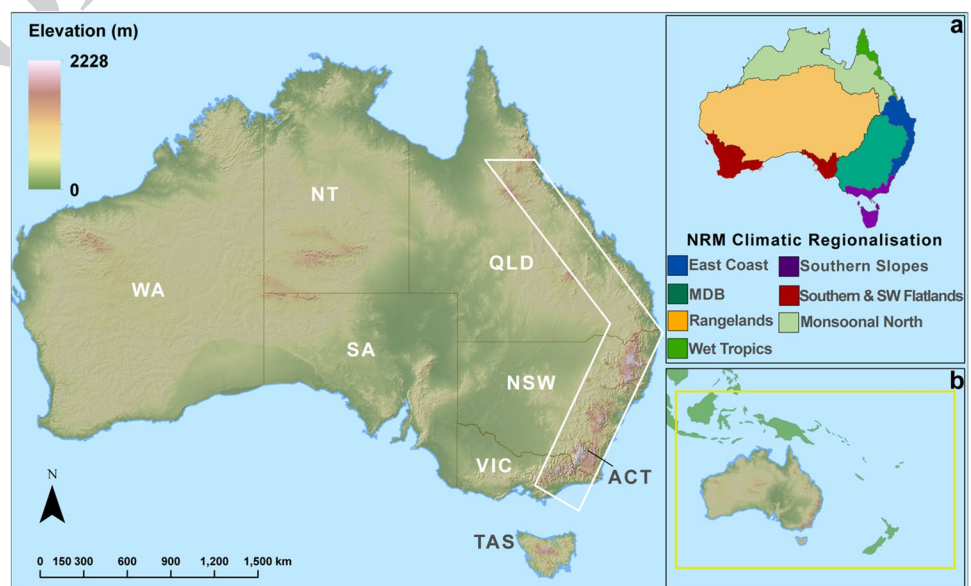


**Table 1** List of CORDEX RCMs analysed and their configurations

Model/version	Responsible institution	Planetary boundary layer physics/surface layer physics	Cumulus physics	Microphysics	Shortwave and long-wave radiation physics	Land surface	Vertical levels
UNSW-WRF360J	University of New South Wales (UNSW)	Mellor-Yamada-Janjic/ETA Similarity	Kain-Fritsch	WRF Double-Moment 5	Dudhia/RRTM	Noah LSM	30
UNSW-WRF360K		Mellor-Yamada-Janjic/ETA Similarity	Betts-Miller-Janjic	WRF Double-Moment 5	Dudhia/RRTM	Noah LSM	30
UNSW-WRF360L		Yonsei University/MM5 Similarity	Kain-Fritsch	WRF Double-Moment 5	CAM3/CAM3	Noah LSM	30
MU-WRF330	Murdoch University	Yonsei University/MM5 Similarity	Kain-Fritsch	WRF Single-Moment 5	Dudhia/RRTM	Noah LSM	30
CCAM	CSIRO	Monin-Obukhov Similarity Theory stability-dependent boundary-layer scheme (McGregor 1993)	Mass-flux closure (McGregor 2003)	Liquid and ice-water scheme (Rotstayn 1997)	GFDL (Freidenreich and Ramaswamy 1999)	CABLE (Kowalczyk et al. 2006)	27
CCLM4-8-17-CLM3-5	Climate Limited-area Modelling Community	Prognostic turbulent kinetic energy (Raschendorfer 2001)	Bechtold et al. (2008)	Seifert and Beheng (2001), reduced to one moment scheme	Ritter and Geleyn (1992)	CLM; (Dickinson et al. 2006)	35



191 (Schrodin and Heise 2001). Further information on the  
 192 dynamics and physical parametrisations in COSMO-CLM  
 193 can be found in Doms and Baldauf (2015). For the present  
 194 simulations, CCLM used a domain with quasi-regular  
 195 grid spacing of approximately 50 km ( $0.44^\circ \times 0.44^\circ$   
 196 on a rotated coordinate system) covering the CORDEX-  
 197 Australasia region. Initial ‘trial’ simulations using the  
 198 standard version of CCLM (CCLM4.8\_clm17) were  
 199 conducted using a number of different model configura-  
 200 tions. These initial simulations showed large temperature  
 201 overestimates over Australia in comparison to observed  
 202 near-surface temperature from the CRU TS 3.10 data set  
 203 (Harris et al. 2014). Subsequent simulations conducted  
 204 using CCLM coupled to the community land model  
 205 version 3.5 (CLM3.5, Dickinson et al. 2006) showed a  
 206 substantial reduction in temperature overestimation. We  
 207 therefore ran the simulations using the coupled model  
 208 CCLM4.8\_clm17-CLM3.5 (CCLM4-8-17-CLM3-5 in the  
 209 CORDEX archive nomenclature). The model parameteri-  
 210 sations used for CCLM are shown in Table 1.

211 The namelists used for all simulations evaluated by this  
 212 study are provided in Online Resource 1. All RCM data  
 213 were interpolated from the models’ native grid to a com-  
 214 mon regular  $0.5^\circ$  grid for comparison and analysis using  
 215 a nearest-neighbour algorithm.

## 2.2 Observations

217 Australian Gridded Climate Data (AGCD; Jones et al. 2009)  
 218 were used to evaluate RCM performance. This daily gridded  
 219 maximum and minimum temperature and precipitation  
 220 data set has a spatial resolution of  $0.05^\circ$ , and is obtained  
 221 from an interpolation of station observations across the Aus-  
 222 tralian continent (Jones et al. 2009). Observations include  
 223 temperature minima and maxima only; hence, the ability of  
 224 RCMs to reproduce mean temperature was not assessed. The  
 225 majority of these stations are located in the more heavily  
 226 populated coastal areas with a sparser representation inland,  
 227 and there are more precipitation stations than temperature  
 228 stations (refer to Fig. 2 of Jones et al. 2009). Cross-validated  
 229 root mean squared errors (RMSEs) for monthly maximum  
 230 and minimum temperatures over Australia for 2001–2007  
 231 are typically between 0.5 and 1 °C, and 10–25 mm month<sup>-1</sup>  
 232 for monthly precipitation (Jones et al. 2009). In order to  
 233 compare models with slightly different spatial resolutions  
 234 with gridded observations of a higher resolution, two dif-  
 235 ferent approaches can be adopted. One is that model output  
 236 can be interpolated to match the higher resolution of the  
 237 gridded observations such that the latter remain unchanged  
 238 (see for example Vautard et al. 2013 and; Zollo et al. 2016).  
 239 However, in our case, the resolution of the observations is  
 240 approximately 10 times higher than that of the models (5 by  
 241 5 km as compared to approximately 50 by 50 km). A major  
 242 issue with using the native resolution of the observations as

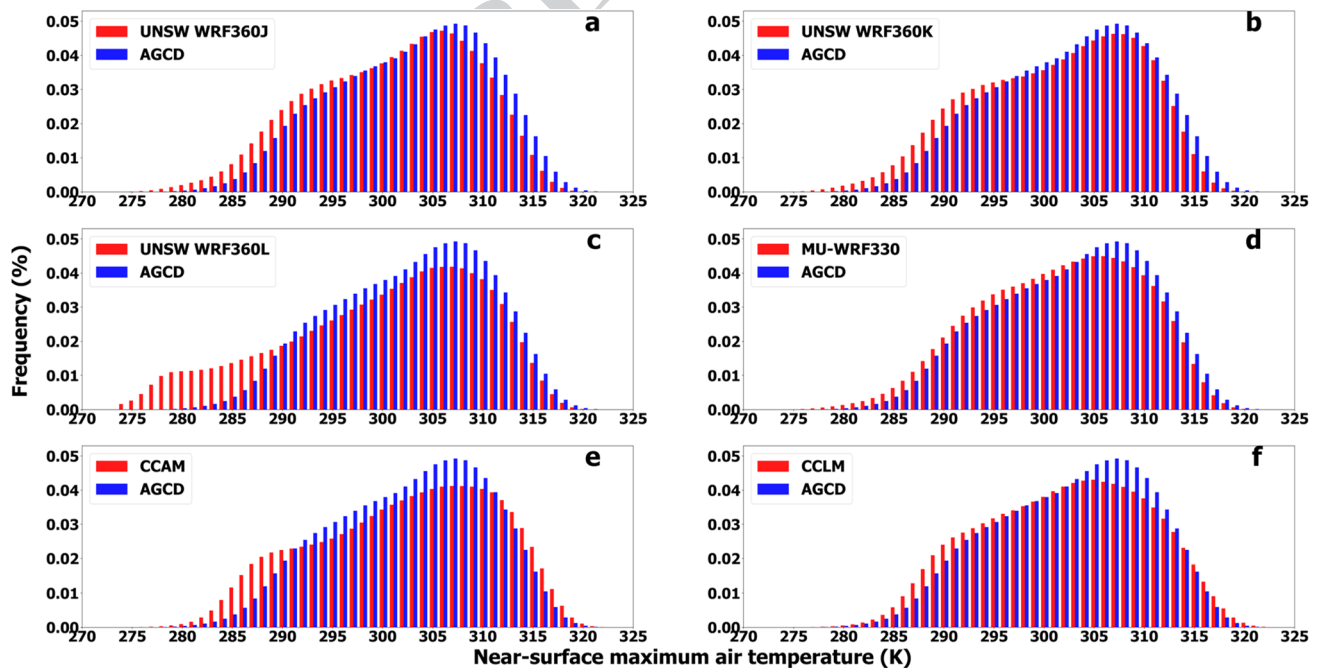


**Fig. 2** Probability density functions of mean daily maximum near-surface air temperatures (K) across Australia. **a–f** The PDF of a specific RCM/ RCM configuration relative to that of Australian Gridded Climate Data (AGCD) observations

the common grid when evaluating lower resolution model output is that statistics with a strong dependence on the spatial scale (particularly extremes) will not be well evaluated. That is, a perfect model at 50 km would disagree with the observations at 5 km resolution, e.g. due to missing small-scale features. Moreover, interpolating the model output to the much higher resolution of the observational grid provides no additional information than the models' original 50 km grid. Of course, when interpolating the observations to a lower resolution the spatial scale mismatch has also to be taken into account. Here, this is handled by using a conservative re-gridding approach. The AGCD data were therefore re-gridded to correspond with the RCM data on a common 0.5° regular grid using the conservative area-weighted re-gridding scheme of the *Iris version 2.1* library (Met Office 2018) for the *Python version 3.6* programming language. Given AGCD observations are terrestrial data with no coverage over the ocean, only land points were evaluated.

### 2.3 Evaluation methods

We calculated annual and seasonal means for maximum and minimum temperature and precipitation using monthly averages for each variable. Mean diurnal ranges and 5th and 95th percentiles were calculated for maximum temperature using daily values. The performance of the RCMs in reproducing the observations over these timescales was assessed by calculating the model bias, defined as model outputs minus AGCD observations. The statistical significance of mean annual and seasonal biases compared to the AGCD observations was calculated for each grid cell using t-tests for maximum and minimum temperature ( $\alpha = 0.05$ ) assuming equal variance. The Mann–Whitney U test was used for precipitation given its non-normality. Results on ensemble mean statistical significance were separated into three classes following Tebaldi et al. (2011). Specifically, statistically insignificant areas are shown in colour, denoting that fewer than half of the models are significantly biased. In these areas model bias is generally small; the most desired outcome. In areas of significant agreement (stippled), at least half of RCMs are significantly biased and at least 66% of the RCMs that show a significant difference agree on the direction of bias. In these regions, ensemble bias tends to be in one direction; an undesirable outcome. Areas of significant disagreement are shown in white, where at least half of the models are significantly biased and fewer than 66% of significant models agree on the bias direction. The 66% threshold was selected because it allowed for a single model to disagree with the consensus.

Model performance against observations was also assessed using the RMSE of simulated fields relative to observations. To evaluate the spatial agreement between RCM outputs and observations, we calculated the pattern

correlation between simulated and observed fields (Walsh and McGregor 1997). The RMSE and pattern correlation were calculated for each RCM using the annual and seasonal means for each variable of interest.

We also examined the ability of the RCMs to simulate observed temperature and precipitation at daily time scales by comparing the probability density functions (PDFs) for AGCD daily mean observations versus those of the RCMs. PDFs were calculated for the whole study domain and for each natural resource management (NRM) climate region shown in Fig. 1. For the PDFs only, all daily values of precipitation below 0.1 mm were omitted from the RCM output, as rates below this amount fall below the detection limit of the stations used to produce the AGCD data. Additionally, the daily rainfall observational network used to produce the AGCD has large gaps in several areas of central Australia; hence, RCM output was masked over these areas. Daily PDFs were compared by calculating the Perkins Skill Score (PSS; Perkins et al. 2007), which measures the common area between two PDFs whereby a PSS value of 1 indicates that the distributions overlap perfectly.

## 3 Results

### 3.1 Maximum temperature

All RCMs overestimate the frequency of lower than average temperatures, as shown by the PDFs of mean daily maximum temperatures across Australia, and underestimate the observed peaks (Fig. 2). The RCMs differ in their simulation of the frequency of warmer than average events, with the four configurations of the WRF RCM underestimating higher temperatures, whereas CCAM and CCLM overestimate occurrences of maximum temperatures higher than 312 K and 314 K, respectively. Overall, MU-WRF330 and CCLM show the best agreement with observations (see PSS scores in Table 2), while the performance of UNSW-WRF360L is comparatively poor. This is generally consistent for the seven NRM climate regions, although the magnitude of the error varies between regions (Fig. 1 and Online Resource 2: Figs. S1–S7).

Ensemble annual mean maximum temperature shows a statistically significant cold bias over most of Australia, which is most intense over the eastern regions (Fig. 3b). Mean bias shows few areas of significant disagreement (white) across Australia, with the majority occurring along portions of the northern and south-eastern coastlines. Additionally, the ensemble mean shows a significant warm bias along sections of the north-western coastline. In terms of individual RCMs, the statistically significant cold bias is the largest for UNSW-WRF360L, which exceeds  $-5$  K over south-eastern Australia (Fig. 3e). UNSW-WRF360L

**Table 2** Perkins skill scores (PSS) for the six RCMs for daily minimum and maximum temperature, diurnal temperature, and daily precipitation

RCM	Temp. max.	Temp. min.	Diurnal range	Precipitation
UNSW-WRF360J	0.94	<b>0.98</b>	0.56	0.76
UNSW-WRF360K	0.94	0.98	0.57	0.69
UNSW-WRF360L	0.88	0.91	0.64	0.72
MU-WRF330	<b>0.95</b>	0.91	<b>0.68</b>	0.76
CCAM	0.90	0.94	0.62	0.76
CCLM	0.95	0.90	0.17	<b>0.78</b>

Bold values indicate the RCM with the highest PSS

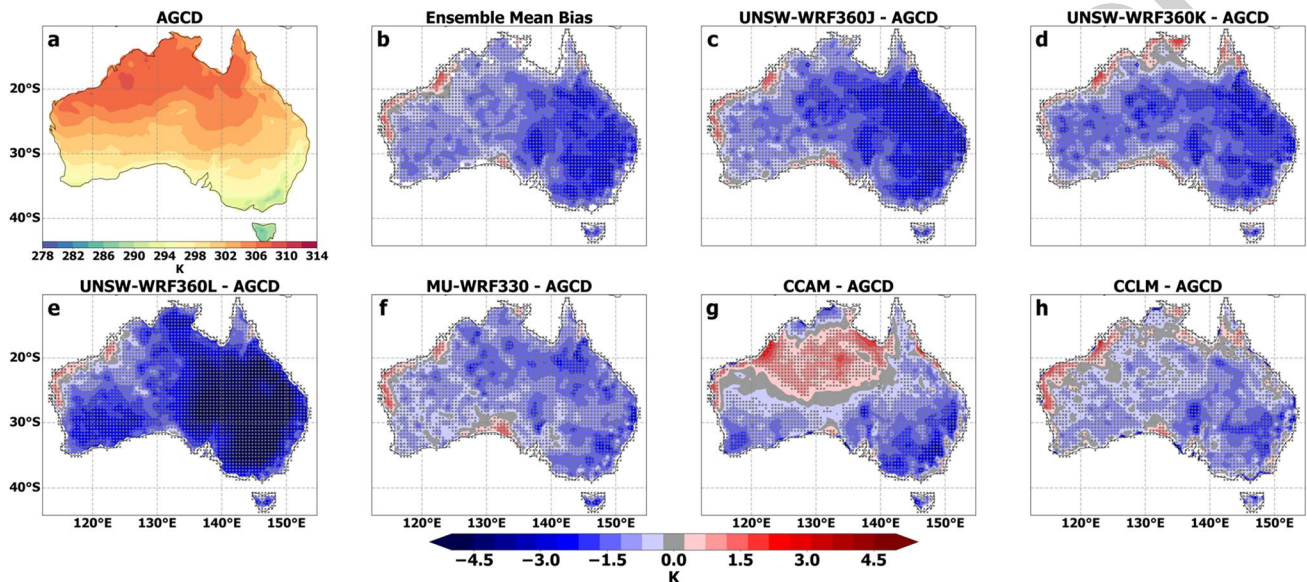


**Fig. 3** Annual mean near-surface atmospheric maximum temperature bias with respect to Australian Gridded Climate Data (AGCD) observations for the RCMs. Stippled areas indicate locations where an RCM shows statistically significant bias ( $P < 0.05$ ). **b** Significance stippling for the ensemble mean bias follows Tebaldi et al. (2011). Statistically insignificant areas are shown in colour, denoting that less than half of the models are significantly biased. In areas of significant

agreement (stippled), at least half of RCMs are significantly biased, and at least 66% of the significant RCMs agree on the direction of the bias. Areas of significant disagreement are shown in white, which are where at least half of the models are significantly biased and less than 66% significant models agree on the bias direction—see main text for additional detail on the stippling regime

343 is exceptional in this regard because other WRF configura- 344  
 344 tions display a substantially smaller cold bias. CCAM 345  
 345 shows a significant warm bias over a larger area as com- 346  
 346 pared to the other RCMs, being 0.5–2.0 K warmer than 347  
 347 observations in the semi-arid areas of central and northern 348  
 348 Australia. Overall, CCLM has the lowest bias.

349 Cold biases are reflected in the spatial variation of 350  
 350 RMSEs for simulated maximum surface temperatures 351  
 351 (Online Resource 2: Fig. S8). For example, UNSW- 352  
 352 WRF360L shows a large area of RMSEs  $> 5$  K over 353  
 353 south-eastern Australia, whilst RMSEs are lower for 354  
 354 CCLM and MU-WRF330 over the most of the continent. 355  
 355 Mean pattern correlations and RMSEs are also consistent 356  
 356 with these results, with CCLM having the lowest RMSE 357  
 357 (0.97 K, versus the ensemble mean of 1.63 K; Table 3) and

MU-WRF330 having the highest mean spatial agreement 358  
 358 between observed and simulated fields. 359

360 At seasonal time-scales, the cold bias tends to be lower in 360  
 360 intensity and spatial extent during summer (DJF, Fig. 4) rela- 361  
 361 tive to during winter (JJA, Fig. 5). This change is the most 362  
 362 apparent for UNSW-WRF360L, which shows a large cold 363  
 363 bias over south-eastern Australia on an annual time-scale 364  
 364 that is greatly reduced during DJF (Fig. 4e). Areas of closer 365  
 365 agreement between simulated and observed temperatures 366  
 366 are also evident across several other regions during DJF, 367  
 367 particularly for the WRF RCM configurations (Fig. 4c–f). 368  
 368 In contrast, most RCMs display larger and more widespread 369  
 369 statistically significant cold biases during the cooler months. 370  
 370 This is most apparent during JJA (Fig. 5); however, CCLM 371  
 371 and to a lesser extent MU-WRF330, do not follow this 372

**Table 3** Diagnostics for six RCMs for annual and seasonal mean minimum and maximum temperature and precipitation for the period January 1981–January 2010 with Australian Gridded Climate Data as reference data

Period	Pearson's <i>r</i>	RMSE												
		UNSW- WRF360J	UNSW- WRF360K	UNSW- WRF360L	MU-WRF330	CCAM	Ensemble Mean	UNSW- WRF360J	UNSW- WRF360K	UNSW- WRF360L	MU-WRF330	CCAM	CCLM	Ensemble Mean
<i>Temp. Max. (K)</i>														
Annual	0.895	0.899	0.869	<b>0.908</b>	0.904	0.903	0.90	1.73	1.55	2.85	1.28	1.37	<b>0.97</b>	1.63
DJF	0.837	0.839	0.856	<b>0.858</b>	0.845	0.841	0.85	1.90	1.66	1.70	1.66	1.77	<b>1.28</b>	1.66
MAM	0.894	0.898	0.858	0.904	0.897	<b>0.906</b>	0.89	2.10	1.95	3.36	2.02	1.86	<b>1.27</b>	2.09
JJA	0.917	0.919	0.817	0.922	0.919	<b>0.925</b>	0.90	2.43	2.23	5.87	1.67	2.18	<b>1.32</b>	2.62
SON	0.906	0.909	0.901	<b>0.915</b>	0.908	0.904	0.91	1.47	1.45	1.77	1.09	1.70	<b>1.04</b>	1.42
<i>Temp. Min. (K)</i>														
Annual	<b>0.902</b>	0.897	0.896	0.900	0.899	0.889	0.90	<b>0.84</b>	0.87	1.57	1.83	1.25	2.33	1.45
DJF	0.908	0.901	0.904	0.909	<b>0.912</b>	0.901	0.91	<b>1.09</b>	1.11	1.19	2.00	1.10	1.84	1.39
MAM	<b>0.896</b>	0.891	0.876	0.894	0.888	0.876	0.89	<b>1.18</b>	1.21	2.02	1.79	1.56	2.62	1.73
JJA	0.855	0.852	0.826	<b>0.856</b>	0.852	0.844	0.85	1.19	<b>1.14</b>	2.95	1.89	2.15	2.86	2.03
SON	<b>0.915</b>	0.909	0.906	0.907	0.915	0.907	0.91	<b>1.03</b>	1.15	1.39	2.29	1.43	2.23	1.59
<i>Prec. (mm month<sup>-1</sup>)</i>														
Annual	0.730	0.630	<b>0.775</b>	0.766	0.712	0.681	0.72	28.00	20.31	18.63	21.64	19.59	<b>15.58</b>	20.62
DJF	0.818	0.753	0.818	<b>0.836</b>	0.789	0.796	0.80	60.93	48.99	51.90	58.89	50.80	<b>37.06</b>	51.43
MAM	0.630	0.547	<b>0.682</b>	0.660	0.611	0.471	0.60	41.65	35.68	35.19	40.10	36.36	<b>26.08</b>	35.84
JJA	0.720	0.715	0.771	0.775	0.788	<b>0.794</b>	0.76	19.89	18.31	15.28	15.72	21.24	<b>11.40</b>	16.97
SON	0.741	0.739	0.803	0.756	<b>0.803</b>	0.752	0.77	30.08	20.82	19.39	21.74	25.01	<b>13.02</b>	21.68

Bold values indicate the RCM with the best diagnostic score



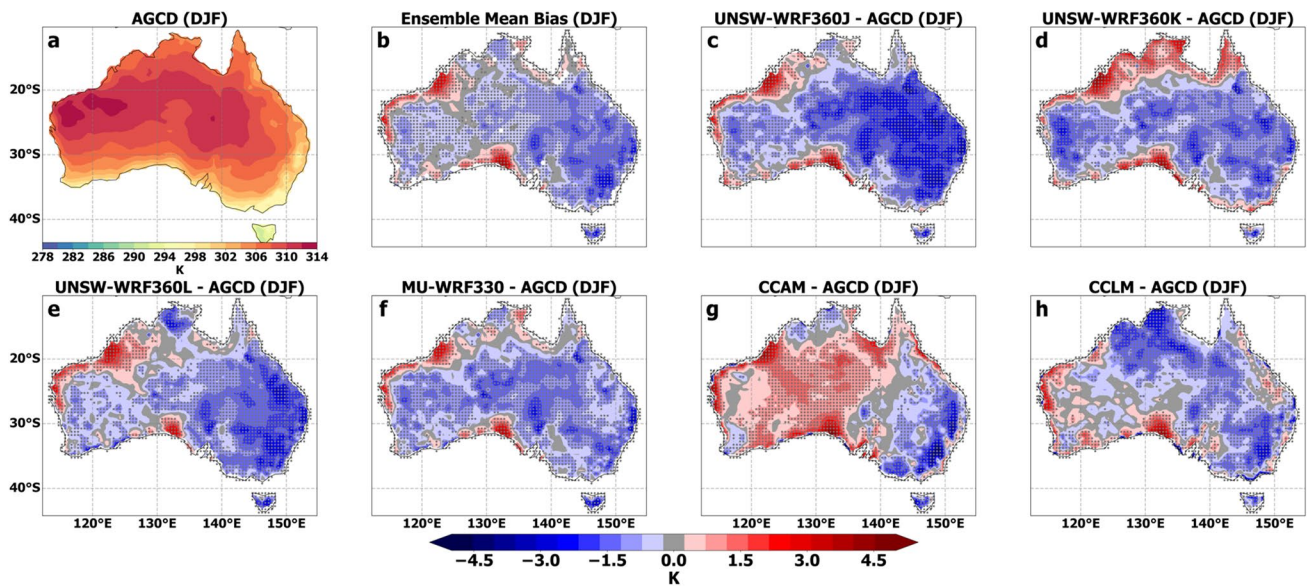


Fig. 4 Summer (DJF) maximum temperature bias with respect to AGCD observations with stippling as per Fig. 3

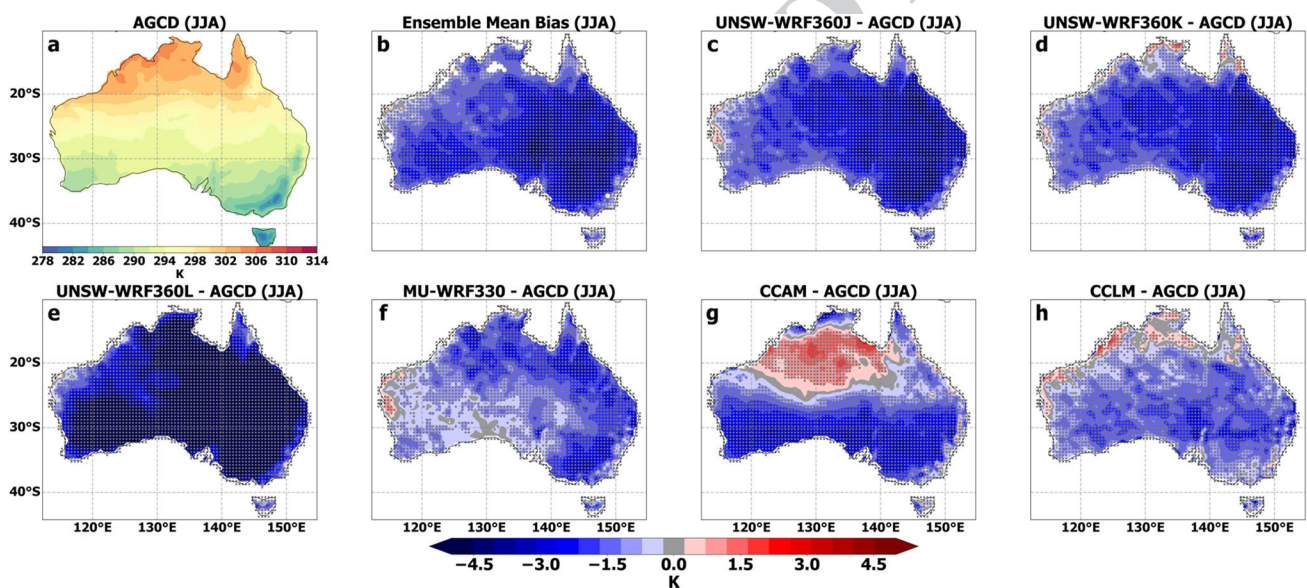
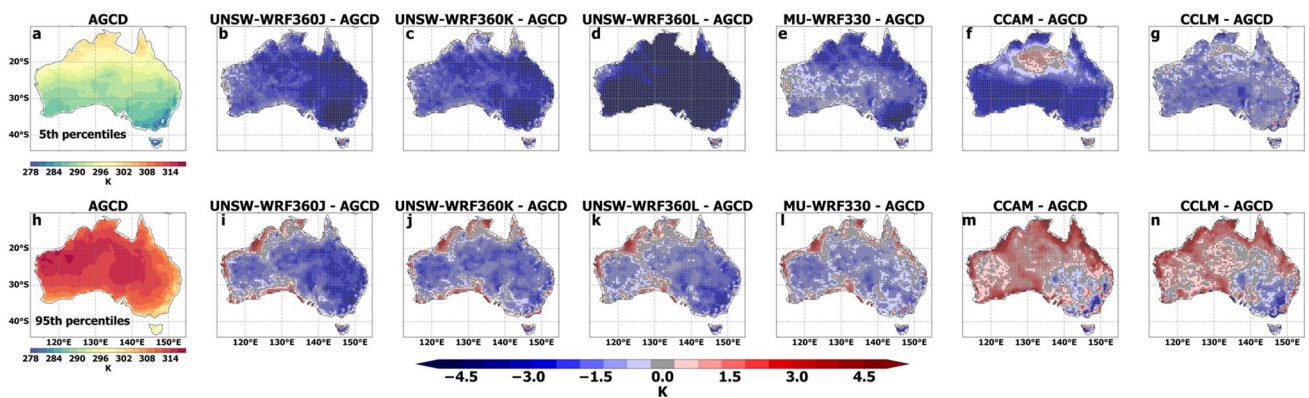


Fig. 5 Winter (JJA) maximum temperature bias with respect to AGCD observations with stippling as per Fig. 3

373 pattern. The poor annual performance of UNSW-WRF360L  
 374 can be attributed to errors during MAM and JJA because  
 375 RMSEs for the model are markedly higher as compared to  
 376 other RCMs during these seasons (Table 3).

377 Figure 6 shows the biases of the 5th and 95th percentiles  
 378 of daily maximum temperature. CCLM shows the  
 379 closest agreement with observed 5th percentile tempera-  
 380 tures. Whereas the RCMs clearly differ in terms of their  
 381 representation of annual and seasonal mean maximum  
 382 temperatures, some similarities are apparent in their simu-  
 383 lation of 95th percentile maximum temperatures. Spatial

patterns of 95th percentile temperature bias are remarka-  
 384 bly similar among the four WRF configurations (Fig. 6i–l),  
 385 and CCAM and CCLM also share very similar patterns of  
 386 bias (Fig. 6m, n). MU-WRF330 shows the lowest bias of  
 387 all WRF RCMs in simulating the 95th percentile across  
 388 the heavily populated south-eastern coastline. Performance  
 389 improves slightly for the WRF RCM configurations when  
 390 simulating 95th percentile maximum temperatures relative  
 391 to annual mean maximum temperatures (i.e. mean RMSEs  
 392 are 1.32 K and 1.85 K respectively; Tables 3, 4).  
 393



**Fig. 6** Biases in 5th percentile (a–g) and 95th percentile (h–n) mean maximum temperatures simulated by the RCMs, relative to AGCD with stippling ( $P < 0.05$ )

### 394 3.2 Minimum temperature

395 Daily minimum temperature PDFs for UNSW-WRF360J and  
 396 WRF360K match observations more closely as compared  
 397 to the other simulations (Fig. 7) and produce the highest  
 398 PSS scores (both scoring 0.98; Table 2). As compared to  
 399 maximum temperatures, these two RCMs show a reduced  
 400 tendency to over (under) estimate the occurrence of tem-  
 401 peratures at the lower (upper) ends of the distribution.  
 402 MU-WRF330, CCAM, and CCLM underestimate the fre-  
 403 quency of colder than average events and overestimate the  
 404 occurrence of warmer than average temperatures. Results  
 405 over specific regions can differ substantially as compared  
 406 to those over the whole of Australia (Online Resource 2:  
 407 Figs. S11–17). For example, in contrast to the Australia-  
 408 wide distribution, both UNSW-WRF360J and WRF360K  
 409 show larger overestimates of the observed peak over the East  
 410 Coast region as compared to the other RCMs.

411 The ensemble annual mean minimum temperature shows  
 412 a statistically significant warm bias for several central and  
 413 eastern regions (Fig. 8b). In contrast to the simulation of  
 414 maximum temperature, all RCMs display significant warm  
 415 bias over larger areas of the topographically complex eastern  
 416 coastline. However, there were some prominent areas of sig-  
 417 nificant disagreement over sections of western and northern  
 418 Australia (Fig. 8b). This can be attributed to MU-WRF330,  
 419 CCAM, and CCLM having significant warm biases across  
 420 most of Australia (Fig. 8f–h), while UNSW-WRF360J-K-  
 421 L show significant cold biases over Western Australia, and  
 422 several northern and eastern regions (Fig. 8c–e). Notably,  
 423 UNSW-WRF360J and WRF360K show closer agreement  
 424 with observed minimum temperatures as compared to the  
 425 other RCMs, with biases typically in the range of  $\pm 1.5$  K  
 426 (Fig. 8c, d), and their performance is considerably improved  
 427 relative to maximum temperatures. These two RCMs have  
 428 the lowest mean RMSEs and low RMSEs across the domain  
 429 (Table 3; Fig. S18).

Seasonally, the spatial variation of the signs and mag- 430  
 nitudes of the biases for each RCM are fairly similar to 431  
 their corresponding performance at the annual time-scale 432  
 (Figs. S19–22). We note that while UNSW-WRF360J and 433  
 UNSW-WRF360K are fairly consistent across seasons in 434  
 terms of mean RMSEs (Table 3), RMSE magnitudes are 435  
 much higher during MAM and JJA for the remaining mod- 436  
 els and in most cases start increasing in March (Online 437  
 Resource 2 Fig. S23). Similar to maximum temperatures, 438  
 the poor annual performance of UNSW-WRF360L can be 439  
 attributed to difficulties in simulating temperatures during 440  
 MAM and JJA (Table 3). 441

### 442 3.3 Diurnal temperature range

All RCMs show relatively poor skill in simulating the 443  
 observed distribution of mean diurnal ranges (Fig. 9). 444  
 Models overestimate the frequency of smaller temperature 445  
 ranges and underestimate the observed peak and occur- 446  
 rence of larger diurnal ranges. UNSW-WRF360L and MU- 447  
 WRF330 perform marginally better than the other RCMs, 448  
 whereas CCLM has the poorest performance (Table 2). 449

The ensemble mean diurnal range bias shows wide- 450  
 spread areas of significant agreement (Fig. 10b); how- 451  
 ever, simulated ranges are generally smaller as compared 452  
 to observed ranges (Fig. 10c–h). The magnitude of this 453  
 negative bias is the largest over eastern Australia; how- 454  
 ever, bias decreases in a westerly direction and in some 455  
 cases its sign is reversed. The ensemble bias shows the largest 456  
 disagreement over southwest Western Australia. Similar 457  
 to seasonal maximum and minimum temperatures, most 458  
 RCMs tend to simulate diurnal ranges more accurately 459  
 during DJF–SON as compared to during MAM–JJA (Figs. 460  
 S24–27). 461



**Table 4** Summary diagnostics for six RCMs when simulating extreme (5th and 95th percentile) maximum and minimum temperature for 1981–2010 using Australian Gridded Climate Data as reference data

Percentile	Pearson's r	RMSE													
		UNSW-WRF360J	UNSW-WRF360K	UNSW-WRF360L	MU-WRF330	CCAM	CCLM	Ensemble Mean	UNSW-WRF360J	UNSW-WRF360K	UNSW-WRF360L	MU-WRF330	CCAM	CCLM	Ensemble Mean
<i>Temp. Max. (K)</i>															
5th	0.93	0.93	0.80	0.80	0.93	0.94	<b>0.94</b>	0.91	2.42	2.21	7.87	1.66	2.24	<b>1.17</b>	2.93
95th	0.87	0.88	<b>0.88</b>	0.87	0.87	0.80	0.85	1.63	1.35	1.26	<b>1.03</b>	1.66	1.38	1.38	1.38
<i>Temp. Min. (K)</i>															
5th	0.88	0.88	0.84	<b>0.89</b>	0.88	0.88	0.87	<b>1.03</b>	1.07	2.85	2.18	2.18	1.72	3.14	2.00
95th	0.90	0.90	0.89	0.90	<b>0.91</b>	0.89	0.90	<b>0.92</b>	0.95	1.04	2.54	1.08	2.19	1.45	1.45

Bold values indicate the RCM with the best diagnostic score

### 3.4 Precipitation

The PDFs for mean daily precipitation show that UNSW-WRF360J and MU-WRF330 simulate the occurrence of light rainfall events up to 0.5 mm day<sup>-1</sup> fairly accurately (Fig. 11). UNSW-WRF360J, MU-WRF330, and CCLM simulate the frequency of precipitation events of  $\geq 3$  mm day<sup>-1</sup> more accurately than the other models. However, the PSS for these models are only marginally higher as compared to the other RCMs with the exception of UNSW-WRF360K (Table 2). There are some interesting differences in RCM performance between regions (Figs. S28–34). For example, light rainfall events (up to 0.5 mm day<sup>-1</sup>) are overestimated by several RCMs over the East Coast, while they are simulated more accurately over the Murray Darling Basin, which is adjacent to the East Coast and further inland.

The ensemble bias for annual mean precipitation shows significant agreement across the eastern, southern, western, and central regions of Australia (Fig. 12b), with areas of significant disagreement occurring mainly over northern Australia and a narrow strip along the eastern coastline. With the exception of MU-WRF330, RCMs show wet biases across large areas of the eastern, central, and southern regions. Some dry biases are also apparent; for example, UNSW-WRF360K, CCAM, and CCLM underestimate rainfall over the monsoonal north, whereas the remaining RCMs display a wet bias in this region. RMSEs are also comparatively high along the northern coastline for all RCMs (Fig. S35). MU-WRF330 displays a wet bias along the eastern coastline, and a dry bias over the lowlands to the west of the Great Dividing Range (Fig. 1) and across the southern half of Australia. Furthermore, MU-WRF330 overestimates rainfall over much of the northern half of Australia and as such, the spatial variation of its bias is an approximate mirror-image to that of CCAM. CCLM has the lowest annual mean RMSE of 15.58 mm month<sup>-1</sup> as compared to the ensemble mean of 20.62 mm month<sup>-1</sup> (Table 3).

Seasonally, many RCMs remain significantly wet-biased over much of eastern Australia, albeit with some regional variations in the sign of the bias. For example, several RCMs show a dry bias over northern regions during DJF, which subsequently switches to a wet bias during MAM, JJA, and SON (Figs. S36–39). The majority of RCMs are better able to capture the spatial pattern of precipitation during DJF, as compared to other seasons or annually, as evidenced by the mean pattern correlations (Table 3). Conversely, when RMSEs are considered, RCMs are most inaccurate during DJF, while accuracy is highest during JJA (Table 3). The strong seasonality of RCM skill is summarised by the RMSE annual cycles in Fig. S40.

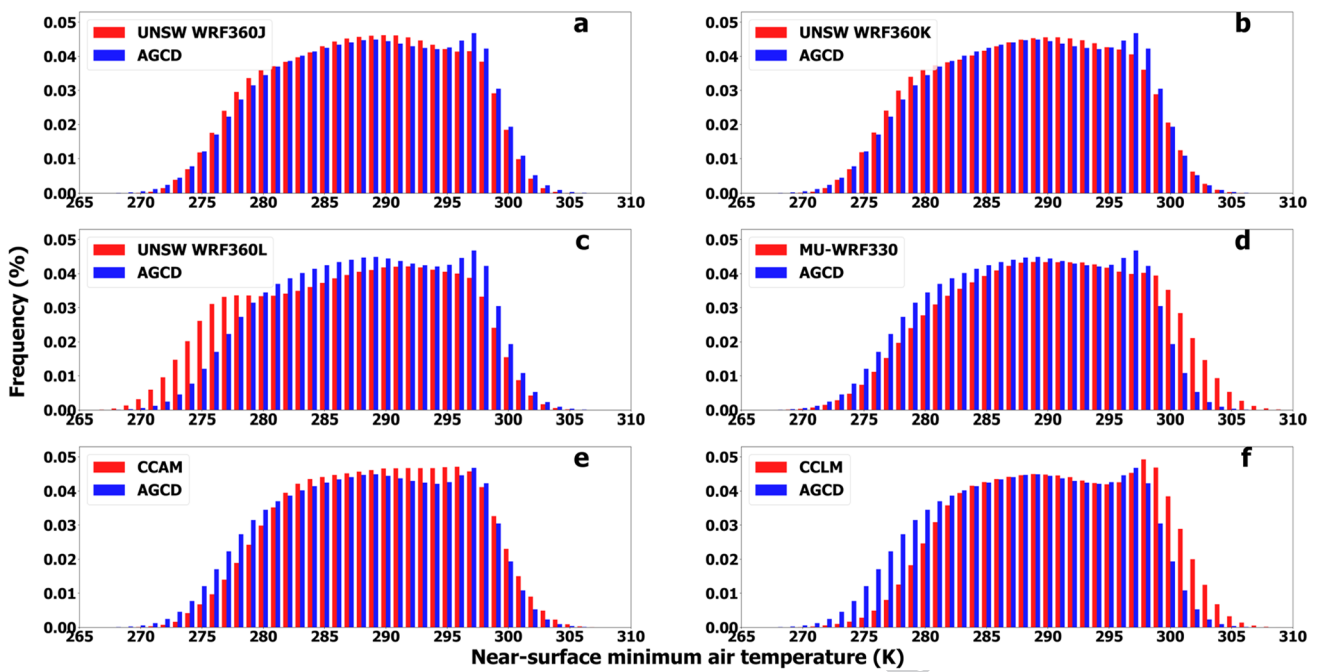


Fig. 7 Probability density functions of mean daily minimum near-surface air temperatures across Australia

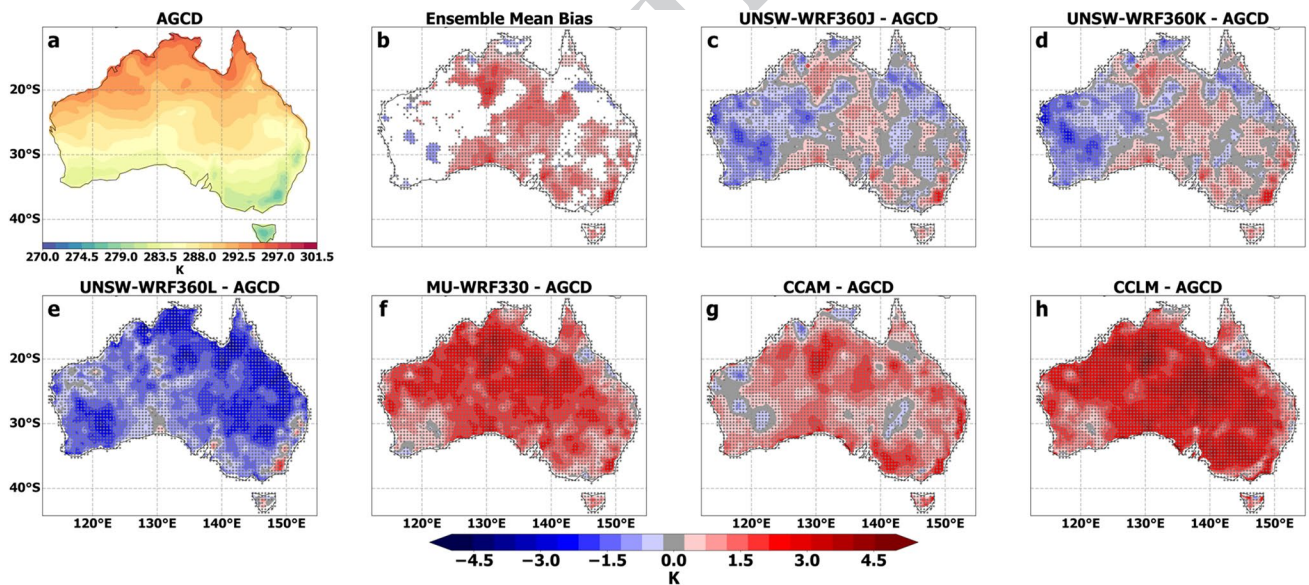


Fig. 8 Annual mean minimum temperature bias (K) with respect to AGCD observations for the RCMs with stippling as per Fig. 3

### 4 Discussion

513

514 In summary, RCMs were generally cold-biased for maxi-  
 515 mum temperature, warm-biased for minimum tempera-  
 516 ture, and overestimated precipitation. However, model

performance varied considerably between seasons and  
 the different RCMs and RCM configurations. The fol-  
 lowing sections discuss potential mechanisms for these  
 differences.

517  
 518  
 519  
 520



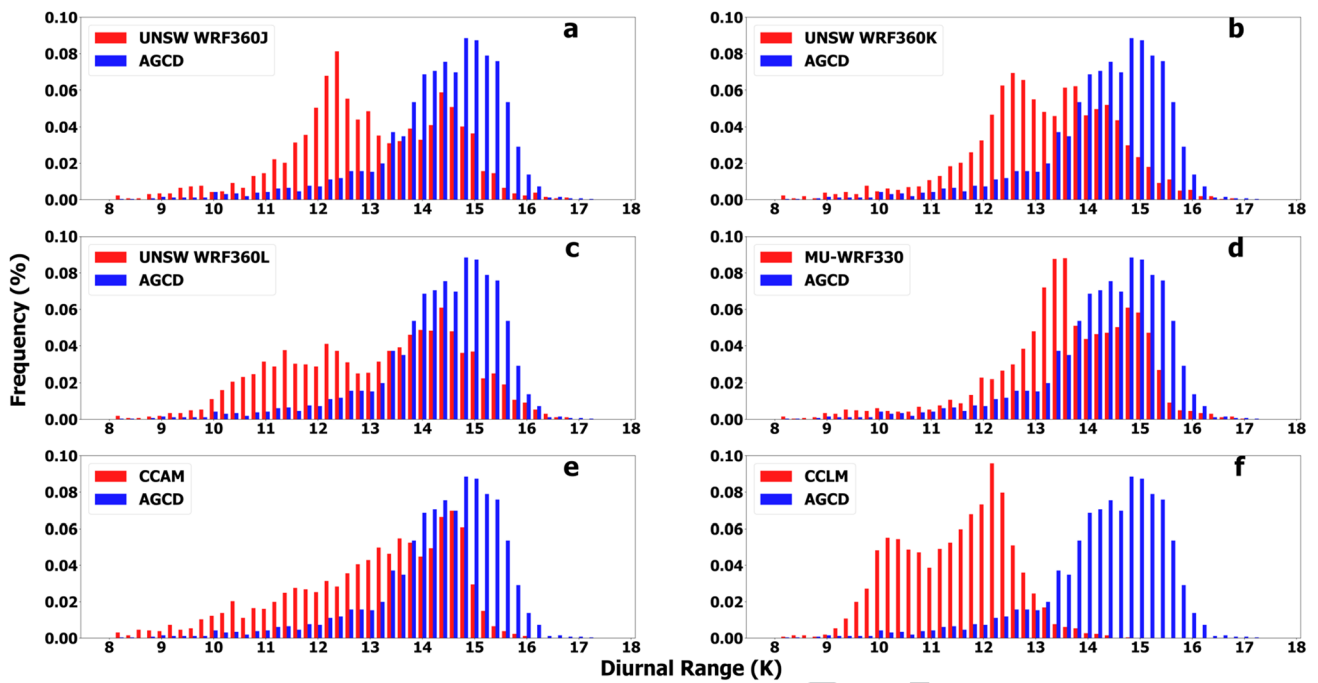


Fig. 9 Probability density functions of mean diurnal ranges across Australia

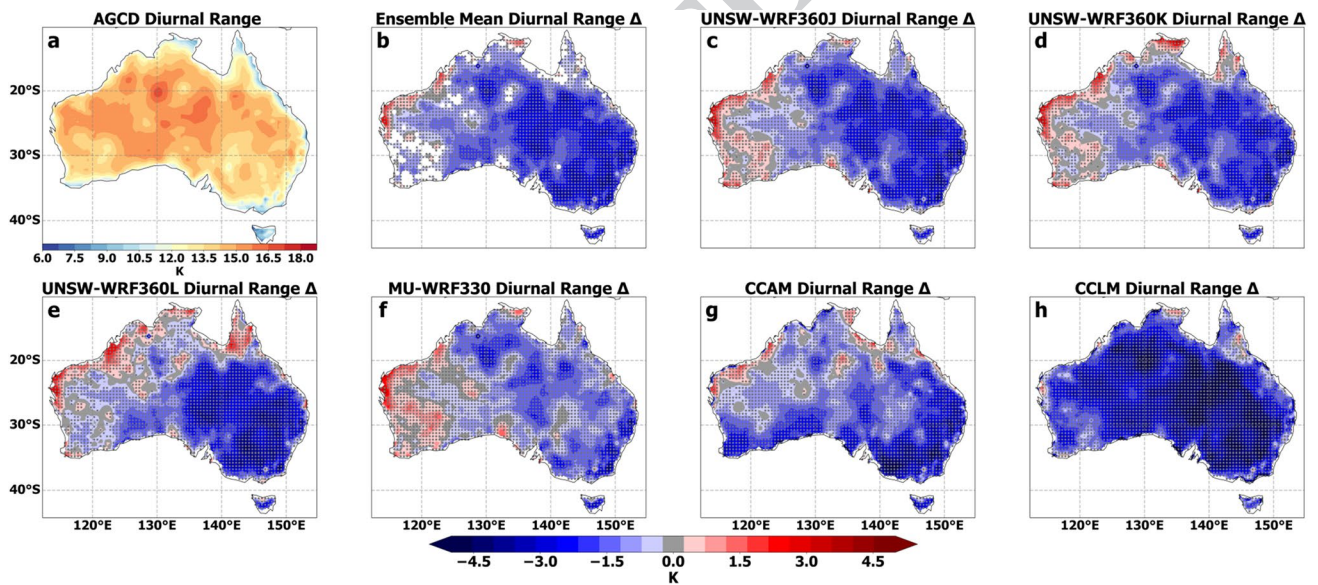


Fig. 10 Bias in the mean diurnal ranges simulated by RCMs relative to observed mean diurnal ranges

521 **4.1 WRF**

522 Cold biases were more widespread and typically larger  
 523 for the four WRF configurations as compared to CCAM  
 524 and CCLM. The unified Noah LSM used by all the WRF  
 525 configurations is a potential source of this bias. Previous  
 526 studies have demonstrated that use of this LSM can result  
 527 in cold biases over European snow-covered regions during

winter and overestimations of soil moisture and evapo- 528  
 ration during summer (Garcia-Diez et al. 2015). While 529  
 snow occupies a small proportion of the land surface in 530  
 south-eastern Australia during cooler months, an excess of 531  
 soil moisture is a potential explanation for the simulated 532  
 cold bias. To investigate this hypothesis, the temporal 533  
 correlation of the 29-year time series between monthly 534  
 biases in precipitation and monthly biases in maximum 535

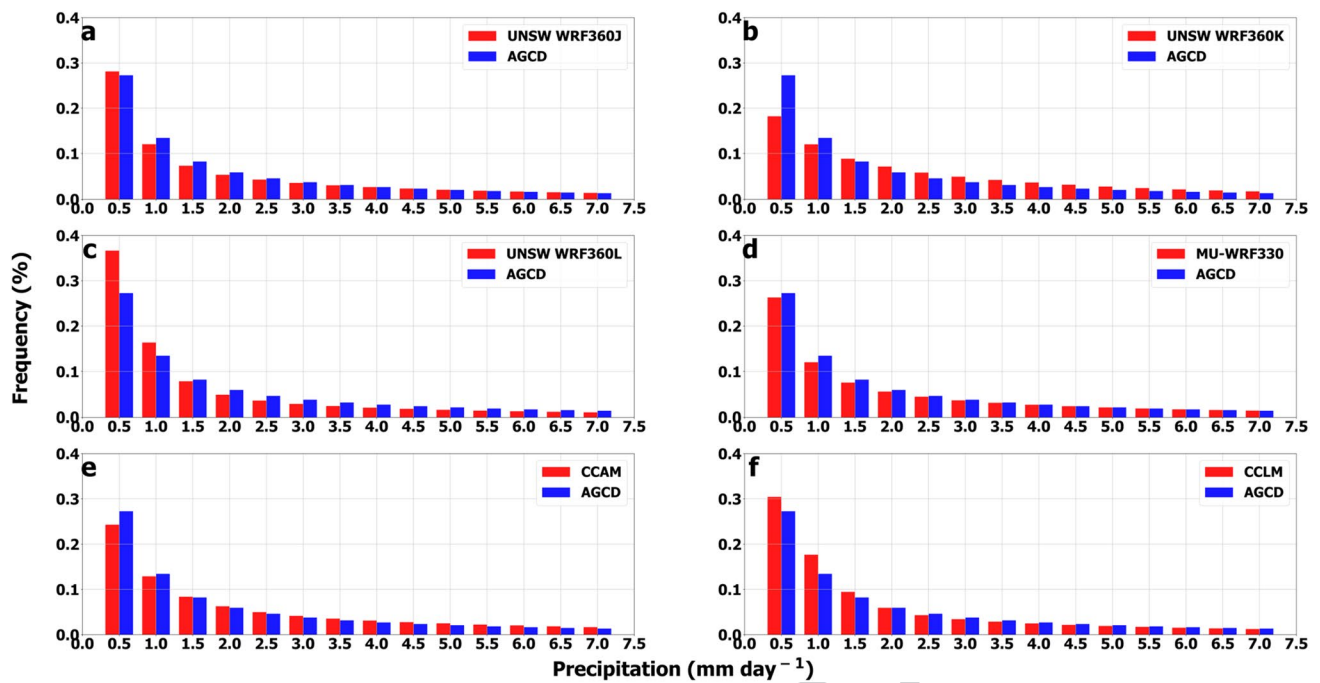


Fig. 11 Probability density functions of mean daily precipitation

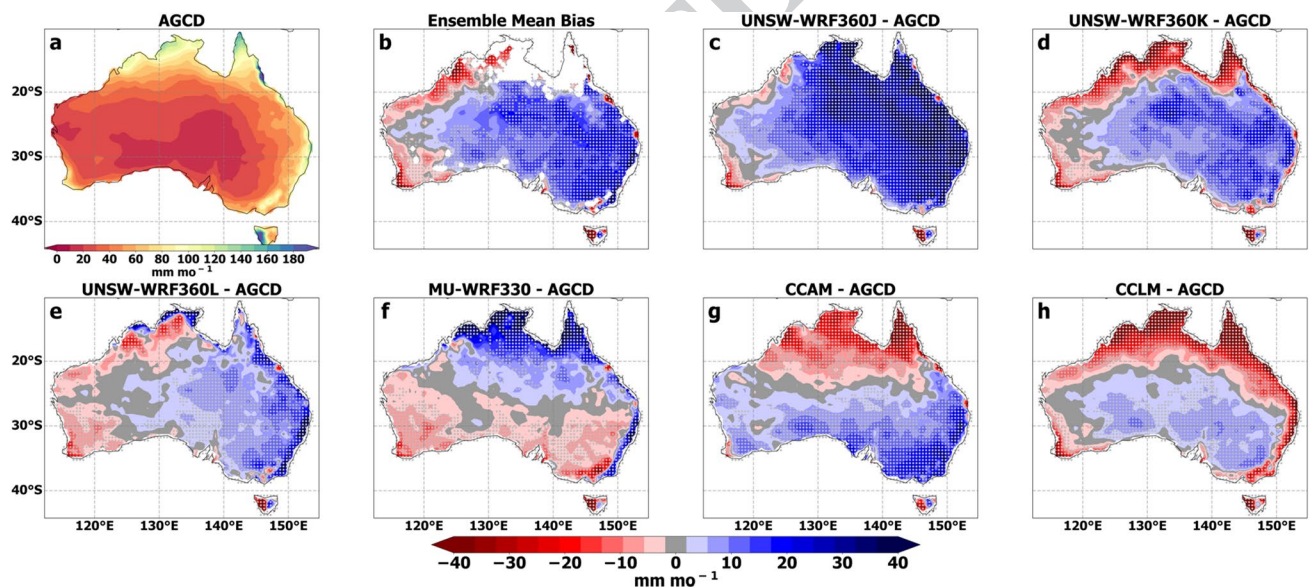
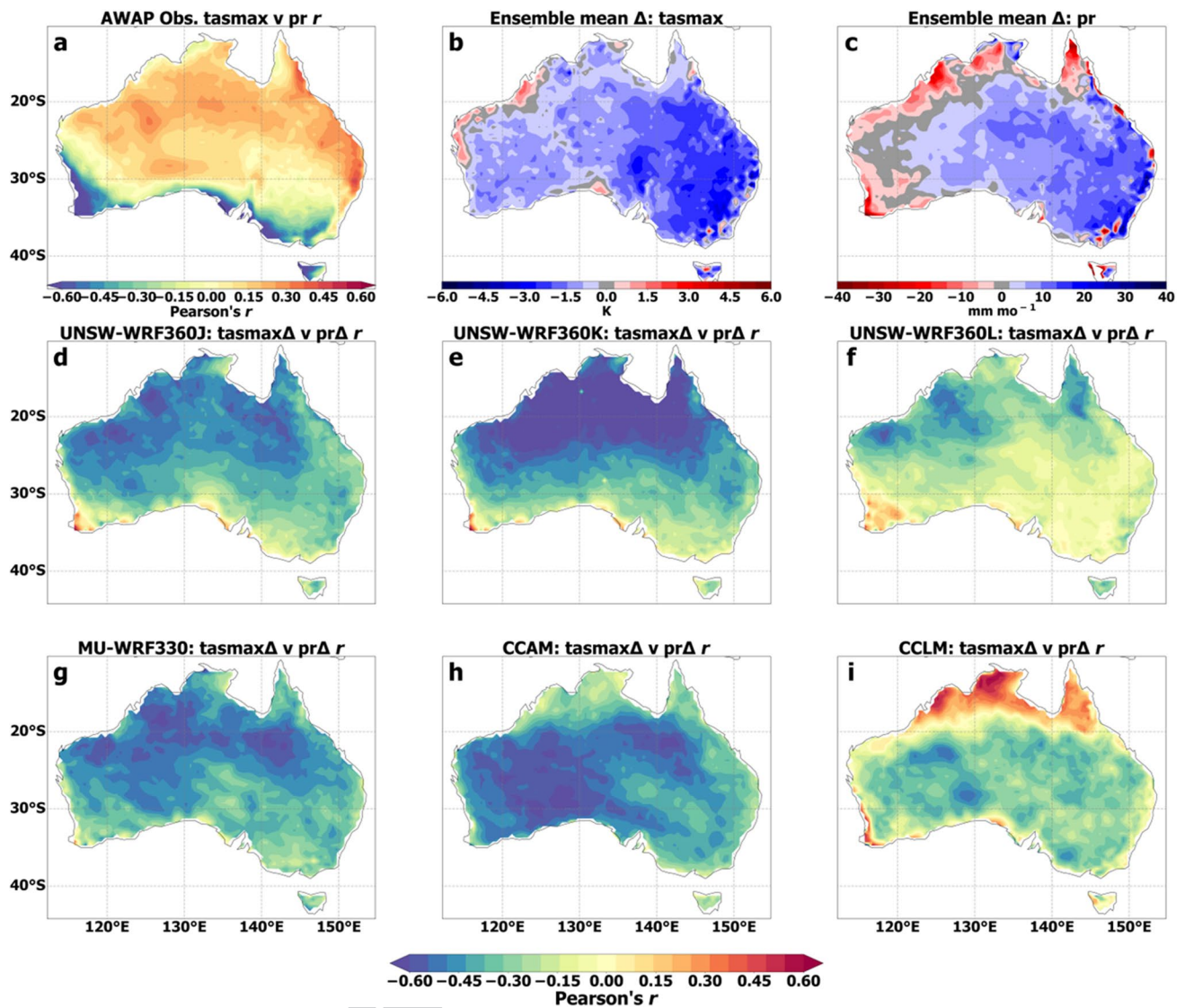


Fig. 12 Annual mean precipitation bias of the RCMs with stippling as per Fig. 3

536 temperature was calculated (Fig. 13). A strong negative  
 537 correlation between mean monthly precipitation biases and  
 538 mean monthly maximum temperature biases was apparent  
 539 over most of Australia. Pearson's  $r$  values averaged across  
 540 Australia for the four WRF configurations ranged from  
 541  $-0.44$  to  $-0.18$ . These associations also displayed strong  
 542 seasonal variability; negative correlations between biases  
 543 were larger and more widespread during DJF as compared

to during JJA (e.g. for UNSW-WRF360J mean  $r = -0.60$   
 versus  $r = -0.18$ , respectively; see Online Resource 2:  
 Figs. S41–S42). These findings support the hypothesis  
 that precipitation overestimation is a likely cause of the  
 large maximum temperature cold bias in the WRF simula-  
 tions. This is consistent with previous studies which have  
 identified Australia as a soil moisture–atmosphere cou-  
 pling “hot spot” for maximum temperature (Hirsch et al.

544  
 545  
 546  
 547  
 548  
 549  
 550  
 551



**Fig. 13** **a** Temporal correlations between observed mean monthly maximum temperature (tasmmax) and precipitation (pr), **b**, **c** biases in modelled versus observed tasmmax and pr, **d–i** temporal correlations between mean monthly biases in maximum temperature and precipitation

2014). Importantly, this negative correlation was reversed for biases in minimum temperature and precipitation (Fig. S43). Moreover, the more accurate simulation of 95th percentile maximum temperatures than annual mean maximum temperatures by the WRF RCM configurations may also be linked to this precipitation bias. Hot extremes in Australia often occur during dry conditions and are hence less affected by the mean precipitation overestimate. Future studies will investigate the drivers of the maximum temperature cold bias using soil moisture observations. Furthermore, since soil moisture is influenced by the LSM, it would also be informative to trial several LSMs with WRF with the aim of improving the representation of land surface processes, and subsequently, the simulation of near-surface temperatures.

The cold bias was more intense for UNSW-WRF360L as compared to other WRF configurations. UNSW-WRF360L was the only configuration to use CAM3 radiation schemes, suggesting that the strong cold bias can be partially attributed to the radiative scheme. This is supported by Katragkou et al. (2015) who also found that using CAM3 resulted in large cold biases.

The WRF configurations showed significant warm biases along portions of the north-western coastline, which were consistent with dry biases over this region. The spatial patterns of 95th percentile maximum temperature bias were also remarkably similar over this region for the four WRF RCM configurations. This consistent north-western bias must be viewed in the context of the relative sparseness of meteorological stations in this region, and the fact that many



stations are located near the coastline where temperatures are lower than further inland. These issues increase the uncertainty of the AGCD observations relative to areas with denser station coverage. The strong relationship between station density and AGCD errors over the north-west and the western interior was noted by Jones et al. (2009), with these regions showing much larger cross-validated RMSEs than elsewhere (see their Figs. 2, 5). Given that other physical settings varied between the different WRF RCMs, it is difficult to identify a specific physical parameterisation that underlies this bias. However, it could also be partially inherited from the ERA-Interim lateral boundary conditions (Moalafhi et al. 2016).

UNSW-WRF360J and WRF360K both showed close agreement with regards to observed minimum temperatures with fairly small biases. This may partially stem from their use of the Mellor-Yamada-Janjic local PBL scheme, which was found to contribute to an accurate simulation of minimum temperature over Southern Spain (Argueso et al. 2011). These two RCM configurations differed only in terms of the cumulus scheme used (UNSW-WRF360J—Kain-Fritsch; UNSW-WRF360K—Betts-Miller-Janjic). Previous sensitivity studies for eastern Australia found that in WRF, these cumulus schemes do not have a large influence on minimum temperature (Evans et al. 2012).

In terms of precipitation biases, similarities between the WRF configurations included dry biases over parts of Western Australia and wet biases over the topographically complex terrain of south-eastern Australia. This south-eastern wet bias changed to a dry bias during winter, which coincides with a substantial improvement in model performance. Rainfall over south-eastern Australia is typically more frequent during the cooler months due to cold fronts moving across southern Australia. These wet biases may be partially inherited from the ERA-Interim lateral boundary conditions, which has a positive precipitation bias over eastern Australia as compared to the Global Precipitation Climatology Centre version 7 observed precipitation (Tuinenburg and de Vries 2017). Most of the model wet biases observed in the present evaluation were largest over eastern Australia. However, despite the fact that the RCMs assessed were driven by ERA-Interim, in many respects they showed quite different patterns of precipitation biases, suggesting that other factors also contributed to this bias. For example, precipitation biases demonstrated by ERA-Interim-forced WRF models over Germany were linked to the models' cumulus scheme not being tuned to European conditions (Warrach-Sagi et al. 2013). While Australia and Germany are very different regions, the cumulus scheme employed by Warrach-Sagi et al. (2013; Kain Fritsch) was used in three of the WRF configurations in the present study. As was the case in Germany, this cumulus scheme was not tuned for Australian conditions. Future work should assess whether using

a higher resolution, such as the 20 km resolution selected for CORDEX2, together with more recent cumulus physics schemes, such as Grell-Freitas (Grell and Freitas 2014) and multiscale Kain-Fritsch (Zheng et al. 2016), will yield precipitation simulations over Australia that are more accurate than the current results.

## 4.2 CCLM

CCLM simulations have been performed over several CORDEX domains (e.g. Africa—Panitz et al. 2014, the Middle East North Africa—Bucchignani et al. 2016 and Europe—Kotlarski et al. 2014). Given that CCLM is based on the COSMO weather forecast model, it has been developed to provide good results for the European domain. For other CORDEX domains, the optimal setup differs from that of the European domain, and also between the various domains. A comparison of results between regions should therefore be performed with caution. The CCLM setup for CORDEX Australasia was based on CORDEX Africa simulations with two major differences. Firstly, the Bechtold et al. (2008) convection scheme was used instead of the Tiedtke (1989) scheme. The former was chosen due to the findings of Lange et al. (2015) who compared both schemes over South America and found that the Bechtold scheme resulted in an improved representation of precipitation. Tests during the setup phase of the present CCLM simulation confirmed that these findings also applied to Australia. Secondly, as described above in Sect. 2.1 Model configurations, the standard LSM, TERRA-ML (Schrodin and Heise 2001), was replaced by CLM3.5 (Dickinson et al. 2006) in order to obtain a better representation of land surface processes.

Although generally cold biased, CCLM resulted in the most accurate representation of maximum temperatures in terms of mean annual and seasonal RMSEs. CCLM showed a maximum temperature bias that was also low, i.e.  $\pm 2$  K across most of Australia. The reasonable results for annual and seasonal mean maximum temperature are partially due to the change of the LSM as described above, which is consistent with previous results for CCLM simulations (e.g. Panitz et al. 2014). Furthermore, we compared the surface solar radiation intensity simulated by CCLM with Surface Radiation Budget (SRB) data (SRB Science Team 2012). This revealed that CCLM simulated lower global radiation (i.e. direct + diffuse solar radiation) and lower net radiation as compared to the SRB data values, a tendency that would lead to lower simulated maximum surface temperatures. However, attribution of the radiation bias shown by CCLM to an overestimation of cloud cover and/or aerosols has not been established. This is because a comparison of observed and modelled cloud cover is not straightforward and requires a tool such as the International Satellite Cloud Climatology Project (ISCCP) data simulator. Hence, an analysis of



cloud cover using satellite measurements of this type merits future investigation. Furthermore, Zubler et al. (2011) and Kothe et al. (2014) found major deficiencies (over Europe and Africa, respectively) when using the aerosol climatology of Tanré et al. (1984) which is the default aerosol climatology used in CCLM. However, both of these studies changed the CCLM program code to accommodate alternative aerosol climatologies to that of Tanré et al., and therefore used unofficial CCLM versions. The Tanré aerosol climatology is the only aerosol scheme implemented in the official released CCLM version 4.18\_clm17 used in the CORDEX-Australia simulations. Therefore, it is not currently possible to conduct sensitivity tests to assess the relationships between different aerosol climatologies and uncertainties in the radiation components. However, in the most recent official version of CCLM (version 5.0), an alternative aerosol climatology can be selected via a namelist setting. An analysis of the influence of aerosol climatology on radiation bias over Australia will therefore be possible for future simulations.

CCLM overestimated the occurrence of warmer than average mean daily minimum temperatures, and overestimated annual mean minimum temperatures by approximately 3–4 K over most of Australia. A comparison of the simulated terrestrial radiation budget to SRB data (SRB Science Team 2012) showed that CCLM overestimated nighttime downward fluxes and also net fluxes, both factors which would contribute to an overestimation of minimum surface temperatures. The combined underestimation of maximum temperatures together with an overestimation of minimum temperatures is one explanation for CCLM's estimates of small diurnal temperature ranges.

CCLM showed fairly close agreement with observed rainfall across the semi-arid inland regions of Australia, whereas it underestimated precipitation across northern Australia and along most of the coastline. This dry bias over coastal areas and tropical Northern regions is consistent with findings by Panitz et al. (2014). The precipitation intensity simulated by CCLM shows a steep gradient between the northern Australian peninsulas and the adjacent ocean areas (not shown). Panitz et al. (2014) stated that "CCLM seems unable to fully transport inland the moisture from the ocean". This may not only affect the water vapor transport, but also the transport of cloud and precipitable water. More recently, Li et al. (2018) observed that precipitation biases shown by CCLM over the CORDEX-East Asian domain were closely linked to biases of water vapor transport. Although the model versions and domains of these studies are different to those of our study, inaccuracy in simulating water vapor transport processes is a possible reason for the precipitation biases observed over some Australian regions. Further investigation is required to understand the causes of the precipitation biases shown by CCLM over Australia, and in particular to test whether they are related to biases in water vapor transport.

### 4.3 CCAM

In contrast to the other models, the CCAM simulation was conducted on a global even/uniform grid and spectrally nudged towards the ERA-Interim data using a scale-selective filter. Hence, the parameterisations were selected to perform well globally and not for a particular region or resolution. In addition, the filter settings used to force the ERA-Interim data were not restrictive (i.e. mainly forcing features with scales larger than 9000 km). Furthermore, CCAM was not constrained by lateral boundary data.

CCAM overestimated occurrences of maximum temperatures at both the lower and upper ends of the observed distribution and was similar to CCLM in this regard. CCAM overestimated maximum temperatures across large regions of northern and central Australia at an annual timescale and during most seasons. Conversely, it was generally cold-biased over the southern half of the country, particularly over the temperate regions of south-western and eastern Australia. Similar to the WRF results, the regions of maximum temperature bias correspond strongly with those of precipitation bias, which suggests that maximum temperature underestimation is related to excessive soil moisture and evaporation and vice versa.

CCAM simulated minimum temperatures more accurately than maximum temperatures. In their evaluation of the current climate of Vietnam, Katzfey et al. (2016) found that CCAM simulated maximum temperatures less accurately than minimum temperatures, which is consistent with our findings. Notably, these results are consistent across very different domains. Although more detailed analysis is required, the CABLE LSM used by CCAM may have some inaccuracies related to the simulation of prescribed soil surface albedo and parameterised vegetation albedo (Wang et al. 2011), issues which would primarily affect the simulation of maximum temperatures.

CCAM's diurnal temperature range PDF, like the observed PDF, has only one major peak, though this peak is shifted slightly towards the lower values. In contrast, the PDFs of the other models show bimodal peaks. The seasonal biases in diurnal temperature are also smaller than those of the other models, except possibly during JJA. Consequently, the CCAM results show a general temperature offset, but a fairly accurate simulation of the diurnal cycle, which could be informative for impact modelling and assessment studies in fields such as agriculture (e.g. Lobell 2007) and human health (e.g. Lambrechts et al. 2011).

CCAM was generally dry-biased over northern regions and wet-biased over the southern half of Australia. However, this northern dry bias was only associated with the wetter seasons (DJF and MAM) because it was reduced during JJA and switched to a wet bias during SON. The CCAM version used by the present study (version 1209)

791 also underestimated precipitation during the Vietnamese  
792 wet season (summer) and overestimated precipitation dur-  
793 ing the dry season (winter) (Katzfey et al. 2016). Similar  
794 to the results reflected in the daily precipitation PDFs of  
795 the present study, CCAM also accurately simulated daily  
796 observed light rainfall events over Vietnam for a threshold  
797 rate of 1 mm day<sup>-1</sup> (Nguyen et al. 2014). Initial experiments  
798 that tested different convection scheme settings showed that  
799 simulated rainfall over tropical regions was sensitive to the  
800 profiles and rates of entrainment and detrainment, which  
801 are configured by various settings in the *kuonml* namelist  
802 options (see Online Resource 1). As described below, exper-  
803 iments that have used updated convection scheme settings  
804 have substantially improved the simulation of rainfall as  
805 compared to the results noted here.

806 The CCAM code evaluated by the present study used a  
807 new prognostic aerosol scheme which overestimated the  
808 concentration of SO<sub>2</sub>. This overestimation of SO<sub>2</sub> concen-  
809 trations would affect CCAM's cloud microphysics (indirect  
810 effects), shortwave radiation (direct effects) and rainfall (via  
811 the number of condensation nuclei). Subsequent refinements  
812 to the CCAM code (version 3355) have alleviated the SO<sub>2</sub>  
813 overestimation issue. Furthermore, additional refinements  
814 have been made to the convective parameterisation and  
815 explicit cumulus scheme, as well as to the CABLE LSM.  
816 More recent simulations that incorporate these refinements  
817 show substantial improvements in the simulation of maxi-  
818 mum and minimum temperatures and precipitation over  
819 Australia (i.e. the magnitudes of biases are substantially  
820 reduced). These model refinements and new results will be  
821 discussed in a future paper.

## 822 5 Conclusions

823 This study evaluated the ability of six reanalysis-driven  
824 RCMs/RCM configurations within the CORDEX Australasia  
825 framework to simulate maximum and minimum tempera-  
826 ture and precipitation over Australia at daily, seasonal, and  
827 annual time scales. In doing so, we address an important  
828 knowledge gap because no such RCM evaluations currently  
829 exist for Australia. RCMs were generally cold-biased when  
830 simulating maximum temperatures over Australia, behaviour  
831 that was particularly characteristic of the WRF RCM con-  
832 figurations. Negative correlations were observed between  
833 mean monthly biases in precipitation and maximum tem-  
834 perature which supports the general conclusion that RCM  
835 cold bias is associated with precipitation overestimation. The  
836 configurations of CCAM and CCLM were quite different to  
837 those of the WRF models. Taking this into account, CCAM  
838 and CCLM performed quite well and offer useful comple-  
839 ments to the WRF configurations assessed. Future refine-  
840 ments to model configurations in the CORDEX Australasia

ensemble that reduce overestimation of precipitation, and  
subsequently soil moisture and evaporation, would improve  
model performance for this region. Since soil moisture is  
influenced by the LSM, it would also be beneficial to test  
different LSMs with the aim of improving the representa-  
tion of land surface processes, and subsequently of surface  
temperatures. Overall, the CORDEX Australasia ensemble  
is valuable for use in further studies. The RCM configu-  
rations assessed here are currently being used to perform  
future climate change projections for Australia, forced by  
GCM outputs from CMIP5. Our assessment of the abilities  
of these RCMs/RCM configurations to simulate Austral-  
ian temperature and precipitation, particularly over heavily  
populated regions, can thus help inform decision-making by  
the adaptation community. Furthermore, the varying model  
capabilities reported here can also help guide experiment  
design and model configuration for climate change impact  
studies over Australia.

**Acknowledgements** We thank the NCAR Mesoscale and Microscale  
Meteorology Division for developing and maintaining WRF. We thank  
Marcus Thatcher and John McGregor at CSIRO Oceans and Atmos-  
phere for developing CCAM, for help with the post-processing software  
to produce the CORDEX output, and for helpful discussions regard-  
ing CCAM. Logistical support was provided by the Climate Change  
Research Centre at the University of New South Wales, by the National  
Computing Infrastructure National Facility at Australian National Uni-  
versity and by the Pawsey Supercomputing Centre. This project is sup-  
ported through funding from the Earth Systems and Climate Change  
Hub of the Australian Government's National Environmental Science  
Programme and the NSW government Office of Environment and  
Heritage. JK is supported by an Australian Research Council (ARC)  
Discovery Early Career Researcher Grant (DE170100102). AD is also  
supported by ARC Grant (DE170101191). RO was supported by the  
Basic Science Research Program through National Research Founda-  
tion of Korea (NRF-2017K1A3A7A03087790), and through the  
Institute for Basic Science (project code IBS-R028-D1). DA received  
funding from the European Union's Horizon 2020 research and innova-  
tion programme under the Marie Skłodowska-Curie Grant agreement  
no. 743547. We thank two anonymous reviewers for their constructive  
feedback on this manuscript.

**Author contributions** JE, AD, RO and DA designed and ran the UNSW  
WRF experiments. JK and JA ran the MU WRF experiments. PH and  
JK ran the CCAM experiment. GD and JE conceived the research  
aims. GD designed and performed the analyses. GD prepared the  
manuscript with contributions from all co-authors.

## 886 Compliance with ethical standards

**Conflict of interest** The authors declare that they have no conflict of  
interest.

## 889 References

Andrys J, Lyons TJ, Kala J (2015) Multidecadal evaluation of WRF  
downscaling capabilities over Western Australia in simulating

- 892 rainfall and temperature extremes. *J Appl Meteorol Climatol*  
893 54:370–394. <https://doi.org/10.1175/jamc-d-14-0212.1>
- 894 Argueso D, Hidalgo-Munoz JM, Gamiz-Fortis SR, Esteban-Parra  
895 MJ, Dudhia J, Castro-Diez Y (2011) Evaluation of WRF  
896 parameterizations for climate studies over Southern Spain  
897 using a multistep. *Region J Clim* 24:5633–5651. <https://doi.org/10.1175/jcli-d-11-00073.1>
- 898 Bechtold P et al (2008) Advances in simulating atmospheric vari-  
899 ability with the ECMWF model: from synoptic to decadal  
900 time-scales. *Q J R Meteorol Soc* 134:1337–1351. <https://doi.org/10.1002/qj.289>
- 901  
902  
903 Bucchignani E, Mercogliano P, Rianna G, Panitz HJ (2016) Analysis  
904 of ERA-Interim-driven COSMO-CLM simulations over Middle  
905 East–North Africa domain at different spatial resolutions. *Int J*  
906 *Climatol* 36:3346–3369. <https://doi.org/10.1002/joc.4559>
- 907 Dee DP et al (2011) The ERA-Interim reanalysis: configuration and  
908 performance of the data assimilation system. *Q J R Meteorol Soc*  
909 137:553–597. <https://doi.org/10.1002/qj.828>
- 910 Di Luca A, de Elia R, Laprise R (2012) Potential for added value in  
911 precipitation simulated by high-resolution nested. *Region Clim*  
912 *Models Observ Clim Dyn* 38:1229–1247. <https://doi.org/10.1007/s00382-011-1068-3>
- 913 Di Luca A, Argueso D, Evans JP, de Elia R, Laprise R (2016) Quanti-  
914 fying the overall added value of dynamical downscaling and the  
915 contribution from different spatial scales. *J Geophys Res Atmos*  
916 121:1575–1590. <https://doi.org/10.1002/2015jd024009>
- 917 Diaconescu EP, Gachon P, Scinocca J, Laprise R (2015) Evaluation  
918 of daily precipitation statistics and monsoon onset/retreat over  
919 western Sahel in multiple data sets. *Clim Dyn* 45:1325–1354.  
920 <https://doi.org/10.1007/s00382-014-2383-2>
- 921 Dickinson RE et al (2006) The community land model and its climate  
922 statistics as a component of the community climate system. *Model*  
923 *J Clim* 19:2302–2324. <https://doi.org/10.1175/jcli3742.1>
- 924 Doms G, Baldauf M (2015) A description of the nonhydrostatic  
925 regional COSMO-Model Part I: dynamics and numerics. DWD,  
926 Offenbach, p 164
- 927 Evans JP, Ekström M, Ji F (2012) Evaluating the performance of a  
928 WRF physics ensemble over South-East, Australia. *Clim Dyn*  
929 39:1241–1258. <https://doi.org/10.1007/s00382-011-1244-5>
- 930 Evans JP, Ji F, Lee C, Smith P, Argüeso D, Fita L (2014) Design  
931 of a regional climate modelling projection ensemble experi-  
932 ment—NARCLiM. *Geosci Model Dev* 7:621–629. <https://doi.org/10.5194/gmd-7-621-2014>
- 933  
934 Fowler HJ, Blenkinsop S, Tebaldi C (2007) Linking climate change  
935 modelling to impacts studies: recent advances in downscaling  
936 techniques for hydrological modelling International. *J Climatol*  
937 27:1547–1578. <https://doi.org/10.1002/joc.1556>
- 938 Freidenreich SM, Ramaswamy V (1999) A new multiple-band solar  
939 radiative parameterization for general circulation models. *J Geophys Res Atmos* 104:31389–31409. <https://doi.org/10.1029/1999JD900456>
- 940  
941 Garcia-Diez M, Fernandez J, Vautard R (2015) An RCM multi-physics  
942 ensemble over Europe: multi-variable evaluation to avoid error  
943 compensation. *Clim Dyn* 45:3141–3156. <https://doi.org/10.1007/s00382-015-2529-x>
- 944  
945 Giorgi F (2006) Regional climate modeling: status and perspectives.  
946 *J Phys IV* 139:101–118. <https://doi.org/10.1051/jp4:2006139008>
- 947  
948 Giorgi F, Bates GT (1989) The climatological skill of a regional  
949 model over complex terrain. *Mon Weather Rev* 117:2325–2347  
950 [https://doi.org/10.1175/1520-0493\(1989\)117%3C2325:tcsoar%3E2.0.co;2](https://doi.org/10.1175/1520-0493(1989)117%3C2325:tcsoar%3E2.0.co;2)
- 951  
952 Giorgi F, Jones C, Asrar G (2009) Addressing climate information  
953 needs at the regional level: the CORDEX framework. *WMO Bull*  
954 53:175–183
- 955 Grell GA, Freitas SR (2014) A scale and aerosol aware stochastic con-  
956 vective parameterization for weather and air quality modeling.  
957 *Atmos Chem Phys* 14:5233–5250. <https://doi.org/10.5194/acp-14-5233-2014>
- Halmstad A, Najafi MR, Moradkhani H (2013) Analysis of precipita-  
tion extremes with the assessment of regional climate models over  
the Willamette River Basin. *USA Hydrol Process* 27:2579–2590.  
<https://doi.org/10.1002/hyp.9376>
- Harris I, Jones PD, Osborn TJ, Lister DH (2014) Updated high-  
resolution grids of monthly climatic observations—the CRU  
TS3.10 Dataset International. *J Climatol* 34:623–642. <https://doi.org/10.1002/joc.3711>
- Hattermann FF, Weiland M, Huang SC, Krysanova V, Kundzewicz ZW  
(2011) Model-supported impact assessment for the water sector in  
Central Germany under climate change—a case study. *Water Resour Manag* 25:3113–3134. <https://doi.org/10.1007/s11269-011-9848-4>
- Hirsch AL, Pitman AJ, Seneviratne SI, Evans JP, Haverd V (2014)  
Summertime maximum and minimum temperature coupling  
asymmetry over Australia determined using WRF. *Geophys Res Lett* 41:1546–1552. <https://doi.org/10.1002/2013GL059055>
- Hoffmann P, Katzfey JJ, McGregor JL, Thatcher M (2016) Bias and  
variance correction of sea surface temperatures used for dynamical  
downscaling. *J Geophys Res Atmos* 121:12877–12890. <https://doi.org/10.1002/2016jd025383>
- IPCC (2012) Managing the risks of extreme events and disasters  
to advance climate change adaptation. In: Field CB, Barros V,  
Stocker TF, Qin D, Dokken DJ, Ebi KL, Mastrandrea MD, Mach  
KJ, Plattner G-K, Allen SK, Tignor M, Midgley PM (eds) A Special  
Report of Working Groups I and II of the Intergovernmental  
Panel on Climate Change. Cambridge, New York
- IPCC (2013) Climate change 2013: the physical science basis. Con-  
tribution of Working Group I to the Fifth Assessment Report of  
the Intergovernmental Panel on Climate Change. Cambridge Uni-  
versity Press, Cambridge. <https://doi.org/10.1017/CBO9781107415324>
- Ji F, Ekström M, Evans JP, Teng J (2014) Evaluating rainfall pat-  
terns using physics scheme ensembles from a regional atmos-  
pheric model. *Theor Appl Climatol* 115:297–304. <https://doi.org/10.1007/s00704-013-0904-2>
- Jones DA, Wang W, Fawcett R (2009) High-quality spatial climate  
data-sets for Australia Aust. *Meteorol Oceanogr J* 58:233–248
- Kala J, Andrys J, Lyons TJ, Foster IJ, Evans BJ (2015) Sensitivity of  
WRF to driving data and physics options on a seasonal time-scale  
for the southwest of Western Australia. *Clim Dyn* 44:633–659.  
<https://doi.org/10.1007/s00382-014-2160-2>
- Katragkou E et al (2015) Regional climate hindcast simulations within  
EURO-CORDEX: evaluation of a WRF multi-physics ensemble.  
*Geosci Model Dev* 8:603–618. <https://doi.org/10.5194/gmd-8-603-2015>
- Katzfey J et al (2016) High-resolution simulations for Vietnam—meth-  
odology and evaluation of current climate. *Asia Pac J Atmos Sci*  
52:91–106. <https://doi.org/10.1007/s13143-016-0011-2>
- King AD, Alexander LV, Donat MG (2013) The efficacy of using grid-  
ded data to examine extreme rainfall characteristics: a case study  
for Australia International. *J Climatol* 33:2376–2387. <https://doi.org/10.1002/joc.3588>
- Kothe S, Panitz HJ, Ahrens B (2014) Analysis of the radiation budget in  
regional climate simulations with COSMO-CLM for Africa. *Meteorol Z* 23:123–141. <https://doi.org/10.1127/0941-2948/2014/0527>
- Kotlarski S et al (2014) Regional climate modeling on European scales:  
a joint standard evaluation of the EURO-CORDEX RCM ensemble.  
*Geosci Model Dev* 7:1297–1333. <https://doi.org/10.5194/gmd-7-1297-2014>
- Kowalczyk E, Wang Y, Law M, L Davies R, Mcgregor HL, Abramowitz  
J G (2006) The CSIRO atmosphere biosphere land exchange  
(CABLE) model for use in climate models and as an offline model  
vol 1615



- 1024 Lambrechts L, Paaijmans KP, Fansiri T, Carrington LB, Kramer LD,  
1025 Thomas MB, Scott TW (2011) Impact of daily temperature fluctu-  
1026 ations on dengue virus transmission by *Aedes aegypti*. Proc  
1027 Natl Acad Sci USA 108:7460–7465. [https://doi.org/10.1073/](https://doi.org/10.1073/pnas.1101377108)  
1028 [pnas.1101377108](https://doi.org/10.1073/pnas.1101377108)
- 1029 Lange S, Rockel B, Volkholz J, Bookhagen B (2015) Regional climate  
1030 model sensitivities to parametrizations of convection and non-  
1031 precipitating subgrid-scale clouds over South America. Clim Dyn  
1032 44:2839–2857. <https://doi.org/10.1007/s00382-014-2199-0>
- 1033 Laprise R (2008) Regional climate modelling. J Comput Phys  
1034 227:3641–3666. <https://doi.org/10.1016/j.jcp.2006.10.024>
- 1035 Li DL et al (2018) Present climate evaluation and added value analysis  
1036 of dynamically downscaled simulations of CORDEX-East Asia. J  
1037 Appl Meteorol Climatol 57:2317–2341. [https://doi.org/10.1175/](https://doi.org/10.1175/jamc-d-18-0008.1)  
1038 [jamc-d-18-0008.1](https://doi.org/10.1175/jamc-d-18-0008.1)
- 1039 Lobell DB (2007) Changes in diurnal temperature range and national  
1040 cereal yields. Agric For Meteorol 145:229–238
- 1041 Maraun D et al (2010) Precipitation downscaling under climate  
1042 change: recent developments to bridge the gap between dynamical  
1043 models and the end user. Rev Geophys 48:34. [https://doi.](https://doi.org/10.1029/2009rg000314)  
1044 [org/10.1029/2009rg000314](https://doi.org/10.1029/2009rg000314)
- 1045 McGregor JL (1993) The CSIRO 9-level atmospheric general circula-  
1046 tion model. CSIRO, Melbourne
- 1047 McGregor JL (2003) A new convection scheme using a simple closure.  
1048 BMRC research report 93. Melbourne, Australia
- 1049 McGregor JL, Dix MR (2008) An updated description of the Con-  
1050 formal-Cubic atmospheric model. In: High resolution numerical  
1051 modelling of the atmosphere and ocean. Springer, New York. [https](https://doi.org/10.1007/978-0-387-49791-4_4)  
1052 [://doi.org/10.1007/978-0-387-49791-4\\_4](https://doi.org/10.1007/978-0-387-49791-4_4)
- 1053 Met Office (2018) Iris: a Python library for analysing and visualising  
1054 meteorological and oceanographic data sets version 2.1. Exeter,  
1055 Devon
- 1056 Moalafhi DB, Evans JP, Sharma A (2016) Evaluating global reanalysis  
1057 datasets for provision of boundary conditions in regional climate  
1058 modelling. Clim Dyn 47:2727–2745. [https://doi.org/10.1007/](https://doi.org/10.1007/s00382-016-2994-x)  
1059 [s00382-016-2994-x](https://doi.org/10.1007/s00382-016-2994-x)
- 1060 Nguyen KC, Katzfey JJ, McGregor JL (2014) Downscaling over Viet-  
1061 nam using the stretched-grid CCAM: verification of the mean and  
1062 interannual variability of rainfall. Clim Dyn 43:861–879. [https://](https://doi.org/10.1007/s00382-013-1976-5)  
1063 [doi.org/10.1007/s00382-013-1976-5](https://doi.org/10.1007/s00382-013-1976-5)
- 1064 Nikulin G et al (2012) Precipitation climatology in an ensemble of  
1065 CORDEX-Africa regional climate simulations. J Clim 25:6057–  
1066 6078. <https://doi.org/10.1175/jcli-d-11-00375.1>
- 1067 Olsson J, Berg P, Kawamura A (2015) Impact of RCM Spatial Resolu-  
1068 tion on the reproduction of local subdaily precipitation. J Hydro-  
1069 meteorol 16:534–547. <https://doi.org/10.1175/jhm-d-14-0007.1>
- 1070 Panitz H-J, Dosio A, Büchner M, Lüthi D, Keuler K (2014) COSMO-  
1071 CLM (CCLM) climate simulations over CORDEX-Africa domain:  
1072 analysis of the ERA-Interim driven simulations at 0.44° and 0.22°  
1073 resolution. Clim Dyn 42:3015–3038. [https://doi.org/10.1007/](https://doi.org/10.1007/s00382-013-1834-5)  
1074 [s00382-013-1834-5](https://doi.org/10.1007/s00382-013-1834-5)
- 1075 Perkins SE, Pitman AJ, Holbrook NJ, McAneney J (2007) Evaluation  
1076 of the AR4 climate models' simulated daily maximum tempera-  
1077 ture, minimum temperature, and precipitation over Australia using  
1078 probability density functions. J Clim 20:4356–4376. [https://doi.](https://doi.org/10.1175/jcli4253.1)  
1079 [org/10.1175/jcli4253.1](https://doi.org/10.1175/jcli4253.1)
- 1080 Raschendorfer M (2001) The new turbulence parameterization of LM.  
1081 COSMO Newsl 1(1):89–97
- 1082 Ritter B, Geleyn J-F (1992) A comprehensive radiation scheme for  
1083 numerical weather prediction models with potential applications  
1084 in climate simulations. Mon Weather Rev 120:303–325
- 1085 Rockel B, Will A, Hense A (2008) The regional climate model  
1086 COSMO-CLM(CCLM). Meteorol Z 17:347–348. [https://doi.](https://doi.org/10.1127/0941-2948/2008/0309)  
1087 [org/10.1127/0941-2948/2008/0309](https://doi.org/10.1127/0941-2948/2008/0309)
- 1088 Rotstajn LD (1997) A physically based scheme for the treatment  
1089 of stratiform clouds and precipitation in large-scale models. I:  
Description evaluation of the microphysical processes. Q J R  
Meteorol Soc 123:1227–1282. [https://doi.org/10.1002/qj.49712](https://doi.org/10.1002/qj.49712354106)  
354106
- Rummukainen M (2016) Added value in regional climate modeling.  
Wiley Interdiscip Rev Clim Chang 7:145–159. [https://doi.](https://doi.org/10.1002/wcc.378)  
org/10.1002/wcc.378
- Schrodin E, Heise E (2001) The multi-layer version of the DWD Soil  
Model TERRA LM. COSMO Technical Report No.2, pp 16,  
Sep 2001, DWD, Offenbach, Germany.
- Seifert A, Beheng KD (2001) A double-moment parameterization for  
simulating autoconversion, accretion and selfcollection. Atmos  
Res 59:265–281. [https://doi.org/10.1016/s0169-8095\(01\)00126](https://doi.org/10.1016/s0169-8095(01)00126-0)  
-0
- Skamarock WC, Klemp JB, Dudhia J, Gill DO, Barker DM, Wang W,  
Powers JG (2008) A description of the advanced research WRF  
Version 3. NCAR Tech Note NCAR/TN-475 + STR. NCAR,  
Boulder
- Solman SA et al (2013) Evaluation of an ensemble of regional cli-  
mate model simulations over South America driven by the ERA-  
Interim reanalysis: model performance and uncertainties. Clim  
Dyn 41:1139–1157. <https://doi.org/10.1007/s00382-013-1667-2>
- SRB Science Team (2012) SRB data. Hampton, VA, USA. [https://doi.](https://doi.org/10.5067/SRB/REL3.1_LW_3HRLY_NC_L2)  
org/10.5067/SRB/REL3.1\_LW\_3HRLY\_NC\_L2
- Sunyer MA, Luchner J, Onof C, Madsen H, Arnbjerg-Nielsen K (2017)  
Assessing the importance of spatio-temporal RCM resolution  
when estimating sub-daily extreme precipitation under current and  
future climate conditions International. J Climatol 37:688–705.  
<https://doi.org/10.1002/joc.4733>
- Tanré D, Geleyn J-F, Slingo J (1984) First results of the introduction  
of an advanced aerosol-radiation interaction in the ECMWF low  
resolution global model. In: Gerber HE, Deepak A (eds) Aerosols  
and their climatic effects. Hampton, Va, p 133
- Tebaldi C, Arblaster JM, Knutti R (2011) Mapping model agree-  
ment on future climate projections Geophys Res Lett. [https://doi.](https://doi.org/10.1029/2011GL049863)  
org/10.1029/2011GL049863
- Thatcher M, McGregor JL (2009) Using a scale-selective filter  
for dynamical downscaling with the conformal cubic atmos-  
pheric model. Mon Weather Rev 137:1742–1752. [https://doi.](https://doi.org/10.1175/2008mwr2599.1)  
org/10.1175/2008mwr2599.1
- Thevakaran A, McGregor JL, Katzfey J, Hoffmann P, Suppiah R,  
Sonnadara DUJ (2016) An assessment of CSIRO conformal  
cubic atmospheric model simulations over Sri Lanka. Clim Dyn  
46:1861–1875. <https://doi.org/10.1007/s00382-015-2680-4>
- Tiedtke M (1989) A comprehensive mass flux scheme for  
cumulus parameterization in large-scale models. Mon  
Weather Rev 117:1779–1800 [https://doi.org/10.1175/1520-](https://doi.org/10.1175/1520-0493(1989)117%3C1779:acmfst%3E2.0.co;2)  
0493(1989)117%3C1779:acmfst%3E2.0.co;2
- Torma C, Giorgi F, Coppola E (2015) Added value of regional climate  
modeling over areas characterized by complex terrain—precipita-  
tion over the Alps. J Geophys Res Atmos 120:3957–3972. [https://doi.](https://doi.org/10.1002/2014JD022781)  
org/10.1002/2014JD022781
- Tuinenburg OA, de Vries JPR (2017) Irrigation patterns resemble  
ERA-interim reanalysis soil moisture additions. Geophys Res Lett  
44:10341–10348. <https://doi.org/10.1002/2017gl074884>
- Vautard R et al (2013) The simulation of European heat waves from  
an ensemble of regional climate models within the EURO-  
CORDEV. Clim Dyn 41:2555–2575. [https://doi.org/10.1007/](https://doi.org/10.1007/s00382-013-1714-z)  
s00382-013-1714-z
- Walsh K, McGregor J (1997) An assessment of simulations of climate  
variability over Australia with a limited area model. Int J Clima-  
tol 17:201–223 [https://doi.org/10.1002/\(sici\)1097-0088\(199702\)](https://doi.org/10.1002/(sici)1097-0088(199702)17:2%3C201::aid-joc118%3E3.3.co;2-r)  
17:2%3C201::aid-joc118%3E3.3.co;2-r
- Wang YQ, Leung LR, McGregor JL, Lee DK, Wang WC, Ding YH,  
Kimura F (2004) Regional climate modeling: progress, chal-  
lenges, and prospects. J Meteorol Soc Jpn 82:1599–1628. [https](https://doi.org/10.2151/jmsj.82.1599)  
://doi.org/10.2151/jmsj.82.1599



- 1156 Wang YP et al (2011) Diagnosing errors in a land surface model  
1157 (CABLE) in the time and frequency domains. *J Geophys Res*  
1158 *Biogeosci* 116:18. <https://doi.org/10.1029/2010jg001385>
- 1159 Warrach-Sagi K, Schwitalla T, Wulfmeyer V, Bauer H-S (2013) Evalu-  
1160 ation of a climate simulation in Europe based on the WRF–NOAH  
1161 model system: precipitation in Germany. *Clim Dyn* 41:755–774.  
1162 <https://doi.org/10.1007/s00382-013-1727-7>
- 1163 Xue YK, Janjic Z, Dudhia J, Vasic R, De Sales F (2014) A review  
1164 on regional dynamical downscaling in intraseasonal to seasonal  
1165 simulation/prediction and major factors that affect downscaling  
1166 ability. *Atmos Res* 147:68–85. <https://doi.org/10.1016/j.atmos>  
1167 [res.2014.05.001](https://doi.org/10.1016/j.atmos)
- 1168 Zheng Y, Alapaty K, Herwehe JA, Genio ADD, Niyogi D (2016)  
1169 Improving high-resolution weather forecasts using the weather  
1170 research and forecasting (WRF) model with an updated Kain–  
1171 Fritsch scheme. *Mon Weather Rev* 144:833–860. [https://doi.](https://doi.org/10.1175/mwr-d-15-0005.1)  
1172 [org/10.1175/mwr-d-15-0005.1](https://doi.org/10.1175/mwr-d-15-0005.1)
- Zollo AL, Rillo V, Bucchignani E, Montesarchio M, Mercogliano P 1173  
(2016) Extreme temperature and precipitation events over Italy:  
1174 assessment of high-resolution simulations with COSMO-CLM  
1175 and future scenarios *International. J Climatol* 36:987–1004. [https](https://doi.org/10.1002/joc.4401)  
1176 [://doi.org/10.1002/joc.4401](https://doi.org/10.1002/joc.4401)
- Zubler EM, Folini D, Lohmann U, Luthi D, Schar C, Wild M (2011) 1177  
1178 Simulation of dimming and brightening in Europe from 1958  
1179 to 2001 using a regional climate model. *J Geophys Res Atmos*  
1180 116:13. <https://doi.org/10.1029/2010jd015396> 1181
- Publisher's Note** Springer Nature remains neutral with regard to 1182  
1183 jurisdictional claims in published maps and institutional affiliations. 1184

UNCORRECTED PROOF